UNIVERSIDAD AUTÓNOMA DE QUERÉTARO
FACULTAD DE MEDICINA
DOCTORADO EN CIENCIAS EN BIOMEDICINA

Análisis *in silico* e *in vitro* del potencial inhibitorio de moléculas sobre los canales SLO3 y CatSper en la funcionalidad del espermatozoide humano

Tesis

Que como parte de los requisitos para obtener el Grado de
Doctor en Ciencias en Biomedicina

Presenta

MC. Jorge Arturo Torres Juárez

Dirigido por:

Dra. Ana Alicia Sánchez Tusie

Ana Alicia Sánchez Tusie
Presidente

Ana Gabriela Hernández Puga
Secretaria

María Carlota García Gutiérrez
Vocal

Esperanza Mata Martínez
Suplente

Claudia Lydia Treviño Santa Cruz
Suplente

Centro Universitario, Querétaro, Qro.
Fecha de aprobación por el Consejo Universitario (26 de noviembre del 2025)
México

Índice

Resumen

Actualmente existe una necesidad insatisfecha de nuevos anticonceptivos masculinos. Para lograr lo anterior, existen: métodos computacionales que permiten acelerar el proceso de desarrollo de fármacos y blancos moleculares validados como el canal CatSper y SLO3. De esta forma, resulta necesario analizar de forma

in silico e *in vitro* los efectos de moléculas con potencial uso de anticonceptivos masculinos sobre la funcionalidad del espermatozoide humano. Metodología: Una vez determinadas las estructuras de los canales CatSper y SLO3 por homología, se identificaron a ligandos potenciales mediante cribado virtual. A continuación, se expusieron dos de estas moléculas a espermatozoides de humano y se determinó su efecto en el potencial de membrana de los espermatozoides, en la motilidad y en la reacción acrosomal. Resultados principales: La alta calidad y validación retrospectiva de los modelos ha permitido identificar potenciales moléculas antagonistas de los canales.

CatSper, SLO3, cribado virtual, anticonceptivos masculinos

Abstract

There is currently an unmet need of new male contraceptives. To achieve this, there are: computational methods that speed up the drug development process and validated molecular targets such as the CatSper and SLO3 channels. Therefore, an *in silico* and *in vitro* analysis of the effects of molecules with potential use in male contraceptives on human sperm functionality is necessary. Methodology: Potential ligands of CatSper and SLO3 were determined by virtual screening using homology models. Human spermatozoa were exposed to two of the selected molecules to determine its effect on membrane potential, motility and acrosomal reaction. Main results: Retrospective validation and high quality of the models have allowed the identification of potential inhibitory molecules.

CatSper, SLO3, virtual screening, male contraceptive

I. Introducción

Los embarazos no planeados generan dificultades socioeconómicas y problemas de salud. Así mismo, dado que la carga de este cuidado recae principalmente en la mujer, resulta necesario aumentar las opciones de anticonceptivos masculinos.

En cuanto a los anticonceptivos masculinos disponibles, solo la vasectomía y el uso de condón han demostrado su efectividad. Sin embargo, la vasectomía no es consistentemente reversible y el condón tiene una tasa anual de fallo considerable. Por estas razones, se requiere un anticonceptivo masculino reversible y efectivo.

Para lograr lo anterior, existen métodos computacionales que permiten acelerar el proceso de identificación de ligandos y su interacción con potenciales blancos. Dentro de estos blancos, se encuentran canales con expresión única en el espermatozoide cuyo correcto funcionamiento es indispensable para la fecundación, como los canales CatSper y SLO3.

Por estas razones, resulta necesario analizar de forma *in silico* e *in vitro* el potencial inhibitorio de moléculas sobre los canales SLO3 y CatSper del espermatozoide humano.

II. Antecedentes

Embarazo no planeado

Los embarazos no planeados son un problema de salud pública que afecta a las mujeres, sus familias y a la sociedad (1). Globalmente, se estima que el 44% de los embarazos son no planificados (2) y, en México, este porcentaje aumenta a 55% (3).

Lo anterior corresponde a 121 millones de embarazos no planeados a nivel mundial (Figura 1) y a 2.1 millones de embarazos no planeados en México. De estos embarazos, cerca del 18% corresponde a embarazo adolescente en México (4), lo que coloca al país en el primer lugar en embarazo adolescente entre los países de la Organización para la Cooperación y el Desarrollo Económico (OCDE) (5).

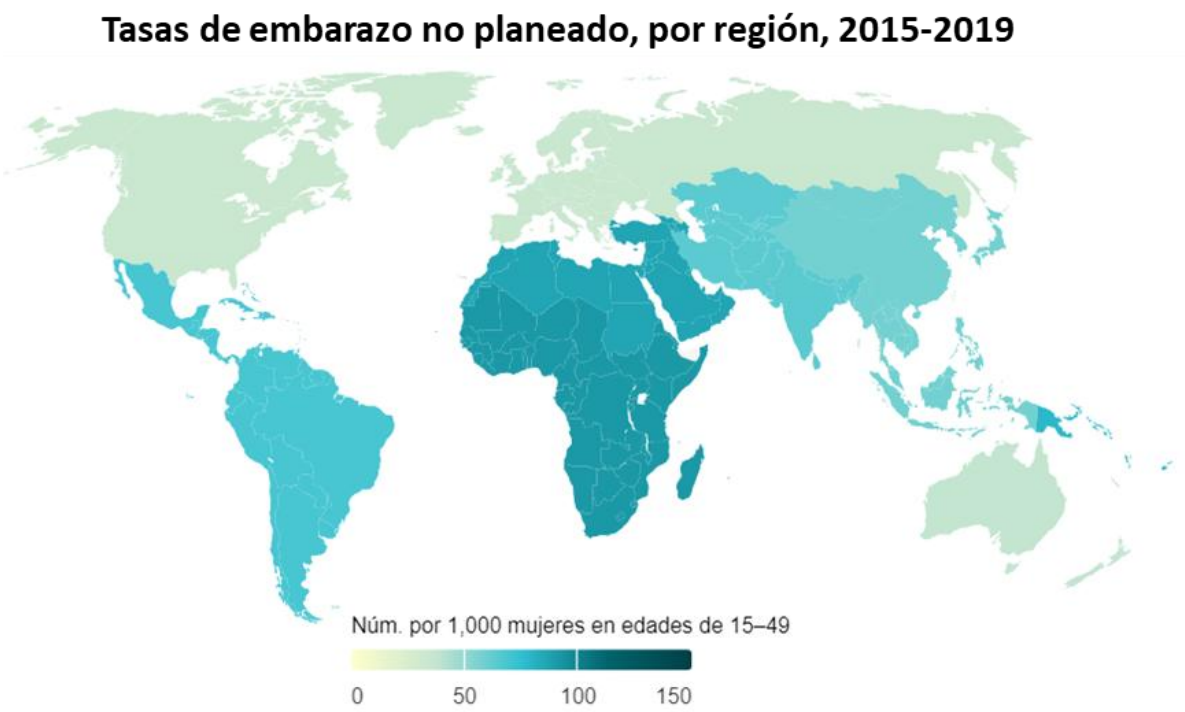

Figura 1. Tasas de embarazo no planeado, por región, 2015-2019. Globalmente, la tasa de embarazo no planeado es de 64 por cada 1000 mujeres en edad reproductiva (15-49). En América Latina y el Caribe, esta tasa aumenta a 69. Tomado de la hoja de datos de Guttmacher – Bearak *et al*., 2020 (2).

Además de su alta prevalencia, los embarazos no planeados impactan negativamente en la salud. Por ejemplo, estos embarazos se han asociado con un aumento en el consumo de drogas durante el embarazo, mayor estrés y depresión materna (6), ausencia de lactancia materna (1), menor desarrollo socioeconómico (7) y muerte materna por aborto.

Así, dado el impacto en la salud de los embarazos no planeados y su alta prevalencia global y nacional, resulta necesario desarrollar nuevas herramientas de planificación familiar.

Métodos anticonceptivos masculinos

Dentro de estas posibles herramientas, una opción atractiva es desarrollar nuevos métodos anticonceptivos ya que la mayoría de los embarazos no planeados son el resultado del fallo anticonceptivo o de la ausencia de su uso (8). En particular, desarrollar nuevos anticonceptivos masculinos promete resolver importantes desventajas de los anticonceptivos masculinos actuales.

Por ejemplo, la vasectomía no es reversible de forma consistente y el condón tiene una tasa de fallo anual del 13% (9). Lo anterior es una posible explicación del bajo porcentaje de uso a nivel mundial, observándose que el condón y la vasectomía son utilizados por el 21 y 2% de los hombres, respectivamente (10).

Aunado a esto, el cuidado de la concepción ha recaído principalmente en la mujer y se ha justificado por la mayor disponibilidad de métodos anticonceptivos femeninos (9). Sin embargo, a pesar de las opciones de métodos anticonceptivos femeninos, dos tercios de las mujeres con embarazos no planeados no usan anticonceptivos o utilizan anticonceptivos poco confiables (9). Siendo una de las razones de su desuso las contraindicaciones o efectos secundarios de estos métodos (11).

Por otro lado, en cuanto a la aceptación hipotética del uso de nuevos anticonceptivos masculinos, entre el 14 y el 83% de los hombres estarían dispuestos a usarlos (12) y más del 70% de las mujeres confiarían este cuidado a su pareja (13). En particular, cerca del 65% de los hombres en México aceptaría usar un nuevo anticonceptivo masculino (14).

De esta forma, existe un interés y una necesidad de desarrollar nuevos anticonceptivos masculinos efectivos y reversibles.

Fertilización

Para lograr lo anterior, se han propuesto diversos métodos en la búsqueda de impedir la fertilización. Este proceso es el último paso de la reproducción sexual y consiste en la unión de los gametos femeninos y masculinos. Los gametos son

células haploides maduras y su fusión genera una célula diploide o zigoto encargada de generar a un nuevo individuo (15).

El gameto femenino es el óvulo y el gameto masculino es el espermatozoide. Ambos gametos son producto de las divisiones meióticas de sus precursores diploides y de los posteriores pasos de desarrollo celular (16). Así, el espermatozoide y sus precursores son blancos de los anticonceptivos masculinos (Figura 2).

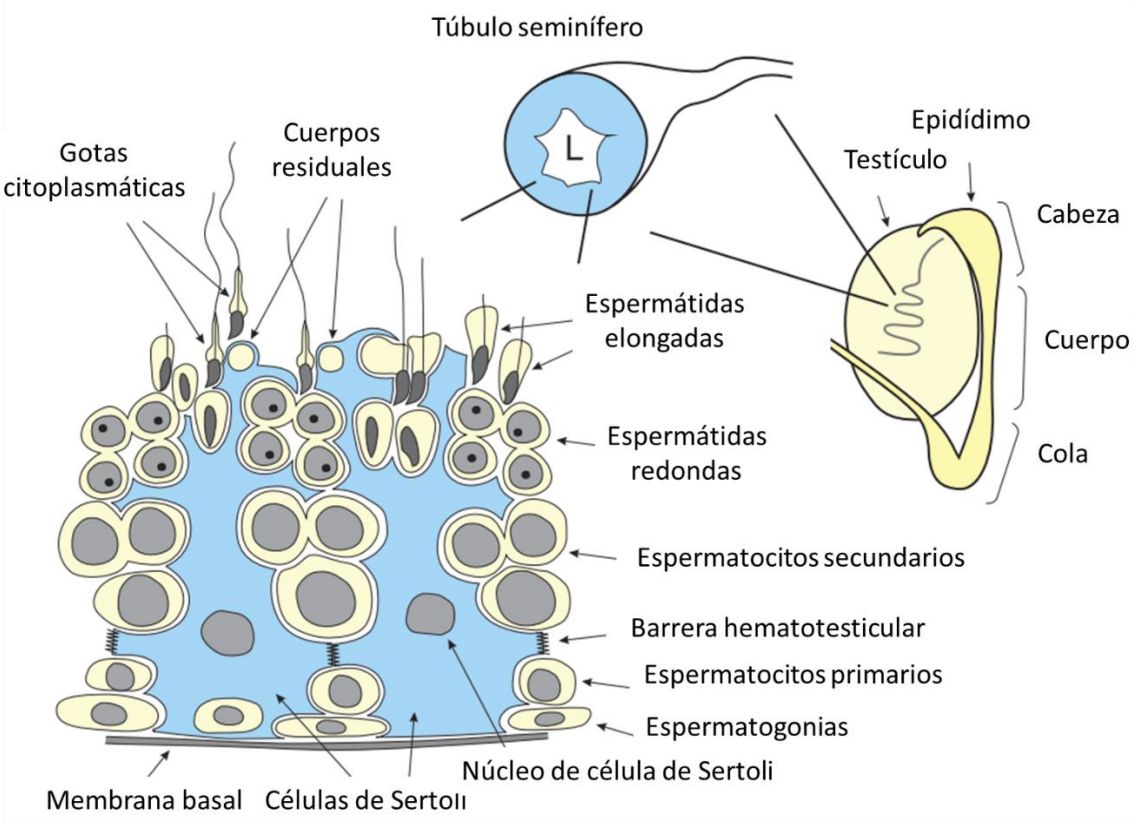

Figura 2. Estructura interna de los túbulos seminíferos y órganos del aparato reproductor masculino. En la imagen de la izquierda se observa la configuración de las células de Sertoli y las fases del desarrollo de los espermatozoides dentro del túbulo seminífero. Del lado derecho se muestra la estructura del testículo y del epidídimo. L: lumen. Imagen modificada de Darszon *et al*. 2011 (17).

Los precursores de los espermatozoides son las espermatogonias y existen dos diferentes clases, A y B. Las A están encargadas de mantener el número de células

germinales mediante mitosis en el proceso de espermatogoniogénesis y las B están encargadas de generar a los gametos. Para esto último, las espermatogonias B se diferencian a espermátidas mediante meiosis en el proceso de espermatogénesis.

Posteriormente, las espermátidas se van a convertir en espermatozoides en el proceso de espermiogénesis. En esta etapa, las espermátidas redondas forman el flagelo, el acrosoma, remueven su exceso de citoplasma y su material genético se supercondensa al sustituir histonas por protaminas (18). De tal forma que estos cambios convierten al espermatozoide en una célula asimétrica y transcripcionalmente inactiva.

Los espermatozoides humanos suelen medir 55-58 micrómetros de largo y están compuestos de una cabeza y una cola. La cabeza es ovalada y alberga tanto al núcleo como al acrosoma. Esta es una vesícula derivada del aparato de Golgi y almacena a enzimas hidrolíticas implicadas en la reacción acrosomal. Por su parte, la cola o el flagelo se divide en la pieza media, en la pieza principal y en la pieza final (19).

Una vez producidos los espermatozoides, estos son liberados hacia el lumen de los túbulos seminíferos (espermiación) para ser transportados por los conductos eferentes hacia el epidídimo. Esta estructura se divide en cabeza, cuerpo y cola y es el lugar en donde los espermatozoides llevan a cabo el proceso de maduración y son almacenados (20).

Los primeros estudios del papel de la maduración epididimal observaron que los espermatozoides adquieren mayor potencial de fertilización mientras más cerca se encontraban de la cola del epidídimo (21,22). Una razón de esto, son los cambios en la motilidad de los espermatozoides, quienes adquieren la capacidad de nadar de forma progresiva en su transcurso a la cola del epidídimo (23).

Posteriormente, en la eyaculación, los espermatozoides maduros son expulsados junto al líquido seminal proveniente de las glándulas accesorias masculinas: las vesículas seminales, la glándula prostática y las glándulas bulbouretrales. Este

conjunto de espermatozoides y líquido seminal recibe el nombre de semen y es depositado en el tracto reproductor femenino durante la reproducción.

Aquí, los espermatozoides llevarán a cabo un segundo proceso de maduración conocido como capacitación espermática (24,25). Este proceso confiere a los espermatozoides la capacidad de realizar la reacción acrosomal y se caracteriza por una serie diversa de cambios fisiológicos y bioquímicos (26). Dentro de estos se encuentran: la remoción del colesterol de membrana plasmática (27), el aumento del pH intracelular (28), el aumento en la fosforilación de tirosinas (29), la hiperpolarización de la membrana (30,31) y la hiperactivación (32).

La hiperactivación consiste en la adquisición de un batido flagelar intenso que permite a los espermatozoides transitar por el oviducto (33,34) y penetrar la zona pelúcida del ovocito (35).

Por su parte, la reacción acrosomal es un proceso exocitótico dependiente de calcio que consiste en la liberación de enzimas hidrolíticas en la proximidad del óvulo (36)(37). Esta reacción les permite a los espermatozoides atravesar las capas externas que rodean al óvulo. De tal modo que, solo los espermatozoides reaccionados pueden fusionarse con el óvulo para depositar su material genético (24).

Métodos hormonales

Cada uno de los anteriores procesos de desarrollo y funciones del espermatozoide son potenciales momentos para la acción de nuevos anticonceptivos masculinos. En cuanto a los métodos hormonales, su objetivo consiste en alterar el proceso de espermatogénesis y el éxito en la intervención se mide por la reducción del número de espermatozoides (38).

Los métodos hormonales funcionan mediante la administración exógena de hormonas sexuales esteroideas, con el fin de provocar la retroalimentación negativa del eje hipotálamo-hipófisis-gonadal (39). De tal forma que estos métodos requieren

aproximadamente dos meses para observar su efecto y el mismo tiempo para revertirlo.

Además de esta restricción, debido a la manipulación del eje endócrino, los anticonceptivos hormonales son capaces de provocar una serie diversa de efectos secundarios, como: reducción de la libido, cambios de humor, obesidad y ginecomastia (39). Debido a lo anterior, existe un interés en generar anticonceptivos no hormonales.

Métodos no hormonales

Dentro de los anticonceptivos no hormonales, los métodos físicos de RISUG/Vasalgel o ADAM consisten en la inyección de polímeros en el conducto deferente (40). Sin embargo, los autores no han demostrado su reversibilidad en humanos (11). Otro método físico es el de Bimek SLV (41). Este es un interruptor implantado para generar el bloqueo del paso de los espermatozoides después de un periodo de tiempo similar al de la vasectomía.

Además del impedimento físico del tránsito de los espermatozoides, otro método físico consiste en elevar la temperatura testicular mediante el uso de ropa interior especial (42). Este instrumento acerca los testículos al cuerpo y requiere usarse la mayor parte del día para observar su eficacia.

Otro enfoque no hormonal es alterar el funcionamiento de proteínas clave del espermatozoide. Una característica buscada en estos blancos es un perfil de expresión exclusivo o principal al tejido testicular y a los espermatozoides. Así, un fármaco selectivo a estos blancos tendría el potencial de evitar efectos secundarios.

Además de su patrón de expresión, otra de las características que fortalecen la relevancia de estos blancos es la evidencia de su indispensabilidad en la reproducción. Por ejemplo, observando los cambios en la capacidad de fertilización al eliminar el gen en modelos animal o en reportes de alteraciones genéticas en humanos.

En el caso de no contar el blanco molecular con una expresión exclusiva en tejido testicular, será la gravedad de los fenotipos presentes la principal limitante para el desarrollo de anticonceptivos dirigidos a estos blancos. Por ejemplo, la adenilato ciclasa soluble se expresa de forma ubicua y la ausencia de su gen se acompaña de elevación en la presión intraocular y propensión a la formación de cálculos renales (43).

Finalmente, otra característica deseable es la evidencia de la capacidad de modular su funcionamiento mediante el uso de diferentes ligandos. Por ejemplo, se han identificado moléculas inhibidoras de CatSper, SLO3, ABHD2, EPPIN, ALDH1A2, BRDT, Slc9cl, TSSK y proteínas de la familia ADAM (40).

De los anteriores blancos moleculares, CatSper y SLO3 son blancos farmacológicos ideales al ser su expresión exclusiva del espermatozoide (44–47) y ser indispensables para la fertilización. Esto se ha observado en la infertilidad reportada en estudios genéticos, tanto en ratones knock-out (44–46,48) como en reportes de alteraciones genéticas en humanos (49,50).

Catsper

CatSper es el principal canal de calcio del espermatozoide y es el canal con el mayor número de subunidades conocido. Las subunidades CATSPER1, 2, 3 y 4 (44–46) son las subunidades formadoras del poro. Cada una de estas posee seis segmentos transmembranales, un filtro selectivo de calcio entre los segmentos transmembranal cinco y seis, y un sensor de voltaje en el segmento transmembranal cuatro (17).

Además de las subunidades formadoras del poro, hasta el momento se han identificado otras 10 subunidades. Dentro de estas, CATSPER beta (51), gamma (52), delta (53) y épsilon (54) son proteínas de membrana con grandes dominios extracelulares. Así mismo, recientemente descubiertas (55), SLCO6C1, CATSPER eta y TMEM249 son proteínas de membrana. Por su parte, EFCAB9, CATSPER zeta y tau son proteínas citosólicas. Dentro de estas, el complejo entre EFCAB9 y CATSPER zeta contribuye a la sensibilidad a pH y calcio del canal (56).

En cuanto a su superestructura, el canal se encuentra ordenado en cuatro dominios discretos, lineales y paralelos en la pieza principal del espermatozoide (57,58). De tal forma que, la señalización de calcio en el espermatozoide se encuentra espaciotemporalmente ordenada.

Finalmente, CatSper es indispensable para la fertilización. Esto se observa en la infertilidad reportada en estudios genéticos, ya sea en modelos de knock-out en ratón (44–46) o en reportes de alteraciones genéticas en humanos (49) .

Lo anterior se explica por el papel de CatSper en el proceso de fertilización. Por ejemplo, los fenotipos de los espermatozoides knock-out de las subunidades de CatSper han implicado al canal en la capacidad de adquirir la hiperactivación durante el proceso de capacitación (59) y en la capacidad del espermatozoide de realizar la reacción acrosomal (60,61). Lo anterior concuerda con la dependencia de estos procesos a la señalización de calcio.

Inhibidores de CatSper

Uno de los puntos que ha favorecido al canal como blanco molecular es la evidencia de su susceptibilidad a la acción de diferentes moléculas. Por ejemplo, Carlson y colaboradores (62) fueron los primeros en reportar a un inhibidor de CatSper (HC-056456). A continuación, dos grupos identificaron al mismo tiempo a NNC55-0396 como inhibidor (63,64) y a Mibefradil (64). Al siguiente año, Brenker y colaboradores (65), reportaron a MDL12330A como inhibidor. Posteriormente, Rennhack y colaboradores (61) reportaron a RU1968 como inhibidor de CatSper. Más recientemente, Rahban y colaboradores reportan la acción bloqueadora de Sertralina (66) y Carlson y colaboradores (67) la acción bloqueadora de ML218. Así mismo, Carlson y colaboradores (68) identificaron 7 series líderes de inhibidores de CatSper mediante cribado de alto procesamiento. Posteriormente, Schierling y colaboradores (69) generaron homólogos de RU1968 y Rehfeld y colaboradores (70) identificaron la acción activadora de CatSper de AM404, compuesto generado a partir de 4-aminofenol, metabolito del paracetamol, y ácido araquidónico. Finalmente, Luque y colaboradores (71) han reportado un nuevo ensayo de alto

procesamiento e identificaron a un posible bloqueador de CatSper dentro de una mini biblioteca de fármacos aprobados por la FDA.

SLO3

SLO3 es el canal principal de potasio del espermatozoide y forma parte de la familia de canales de potasio gran conductancia (BK, SLO o Maxi-K) (72). El canal es un homotetrámero, en donde cada subunidad cuenta con seis segmentos transmembranales y tres dominios: el dominio de poro, el sensor de voltaje y el sensor citosólico a pH (73).

Respecto a su función, el canal está implicado en la generación de la hiperpolarización de la membrana, al facilitar la salida de potasio en el espermatozoide. En el humano, el canal SLO3 es sensible a los cambios de pH y a las concentraciones de calcio. En cambio, en el ratón, el canal es solamente sensible al pH (74).

Existen diferentes subunidades auxiliares para los canales de la familia SLO. Por ejemplo, las propiedades cinéticas y farmacológicas de SLO1 son modificadas por las subunidades beta. Por su parte, la subunidad auxiliar conocida de SLO3 es gama2, y su coadministración en sistemas heterólogos facilita su expresión y modifica sus propiedades electrofisiológicas.

Inhibidores de SLO3

Debido a la dificultad de expresar únicamente las subunidades alfa de SLO3, Tang y colaboradores (75) estudiaron sus propiedades farmacológicas en construcciones quiméricas de SLO3 de ratón (SLO3m). Para esto, emplearon inhibidores conocidos de SLO1 de ratón como quinina, quinidina, carbdotoxina, slotoxina e iberiotoxina.

A partir de los anteriores resultados, Mannowetz y colaboradores (76) investigaron la acción de estos inhibidores en el espermatozoide humano. Al observar la inhibición de la corriente principal de potasio empleando inhibidores de SLO1m, pero no de SLO3m quiméricos, los autores concluyeron que esta corriente dependía principalmente de SLO1.

Sin embargo, esta afirmación se puso en duda al observar que inhibidores no específicos de SLO3m inhibían la corriente y que, en cambio, inhibidores de SLO1m no inhibían la corriente de potasio del espermatozoide. Para esto, Brenker y colaboradores (77) coexpresaron de forma heteróloga al canal SLO3h y a la subunidad gama2 en células CHO. De esta forma, los autores concluyeron que SLO3 es el canal principal de potasio en el espermatozoide humano.

Esta afirmación se fortaleció con los resultados de Sánchez-Carranza y colaboradores (72). En este trabajo, los autores observaron la inhibición de la hiperpolarización de la membrana en los espermatozoides y la inhibición de la corriente de potasio en células transfectadas con SLO3+gama2 empleando iberiotoxina, slotoxina y carbdotoxina, inhibidores de canales SLO. Así mismo, los autores demostraron diferencias en las propiedades farmacológicas entre SLO3m y SLO3h. Por ejemplo, que la iberiotoxina inhibe parcialmente a SLO3h.

Finalmente, empleando un cribado de alto procesamiento de 50,000 moléculas, Lyon y colaboradores identificaron a un inhibidor selectivo de SLO3h (72). Con este inhibidor, los autores lograron establecer el papel principal de SLO3 en el flujo de potasio, en la hiperpolarización de la membrana del espermatozoide humano, en la hiperactivación y en la reacción acrosomal.

Métodos computacionales

Los avances en la identificación de inhibidores de estos canales han sido facilitados por el desarrollo de ensayos de alto procesamiento. Estos ensayos consisten en registrar el movimiento de los iones o el cambio del potencial de membrana empleando marcadores fluorescentes una vez que se ha estimulado la apertura de los canales. La ventaja de estos ensayos reside en poder estudiar el comportamiento de miles de moléculas de forma más rápida y sencilla. Así, la confirmación mediante electrofisiología se limita a un número reducido de potenciales inhibidores.

Sin embargo, a pesar de estas ventajas, la identificación de inhibidores es una cuestión de serendipia, lo que repercute en el tiempo de identificación y en el costo. De este modo, existe una necesidad de implementar metodologías que reduzcan el espacio y tiempo de búsqueda de nuevos fármacos, como el diseño de fármacos asistido por computadora.

El diseño de fármacos asistido por computadora es un conjunto de técnicas computacionales que tienen el fin de identificar, optimizar y analizar fármacos (79). Dentro de estas técnicas, el modelado por homología, el acoplamiento molecular, el cribado virtual y la dinámica molecular son opciones que se han utilizado con éxito para traer nuevos fármacos al mercado (80).

El modelado por homología es una técnica computacional para la generación de estructuras tridimensionales de las proteínas blanco. En esta técnica, se utiliza la estructura tridimensional conocida de un homólogo de la proteína blanco como molde. Así, a mayor porcentaje de identidad entre estas secuencias existe una menor ambigüedad en la estructura del modelo. Como regla general, un 30% de identidad se considera suficiente para la generación de un modelo teórico (81).

El acoplamiento molecular es una técnica de evaluación de la interacción entre una molécula y el receptor blanco (82). Para esto, los algoritmos de acoplamiento generan diferentes modelos de unión ligando-receptor. Así mismo, estos algoritmos utilizan una función de puntaje para evaluar la fuerza de interacción de cada modelo generado.

En la generación de complejos ligando-receptor, el acoplamiento puede ser de dos tipos: rígido o flexible. En el caso del acoplamiento rígido, el receptor y el ligando permanecen en su conformación original por lo que la búsqueda de complejos se limita a rotar y trasladar al ligando en el sitio de unión. Por otro lado, el acoplamiento flexible permite el movimiento de las cadenas laterales del receptor y de los enlaces rotables del ligando. De esta forma, el número de posees exploradas aumenta, aunque también lo hace el costo computacional (83).

Por su parte, el cribado virtual es la técnica computacional que compara y ordena a diferentes moléculas de acuerdo a alguna medida del grado de afinidad al receptor blanco (84). Por ejemplo, para el cribado virtual basado en ligandos, el grado de afinidad de las moléculas constituye el grado de similitud de la estructura de estas moléculas con ligandos conocidos. En cambio, en el cribado virtual basado en la estructura, el grado de afinidad es igual al puntaje de acoplamiento molecular.(85). A pesar de esta distinción, existen protocolos validados que combinan ambos métodos (86). De esta forma, el cribado virtual permite acelerar el proceso de identificación de potenciales ligandos y su interacción con las moléculas objetivo (87).

Métodos computacionales en el desarrollo de anticonceptivos masculinos

Estos métodos computacionales han sido utilizados con éxito en diferentes etapas del desarrollo de anticonceptivos masculinos. Por ejemplo, EPPIN es una proteína de la superficie del espermatozoide y la inhibición de su unión a SMEG1, proteína formadora del gel seminal, genera infertilidad. En este caso, durante el proceso de optimización de inhibidores de EPPIN, se modelaron y acoplaron molecularmente segmentos de SEMG1 con el fin de identificar el sitio de interacción EPPIN-SEMG1 (88).

De forma similar, se han realizado cribados virtuales de alto procesamiento para la identificación de inhibidores de BRDT, regulador transcripcional y epigenético esencial para la espermatogénesis (89).

Más recientemente, se han realizado acoplamientos moleculares para la identificación de análogos de ER-50891, antagonista selectivo del receptor de ácido retinoico alfa, y la identificación de YCT529 (90) compuesto que está siendo evaluado por primera vez en ensayos clínicos (ClinicalTrial.gov ID: NCT06094283).

Así, los anteriores estudios son evidencia del potencial de implementar estos métodos en la búsqueda de nuevos anticonceptivos masculinos. Por ejemplo, para la identificación de nuevos inhibidores de CatSper y SLO3 existen estructuras tridimensionales de canales homólogos de estos blancos moleculares. Estas

estructuras se resolvieron mediante crio-microscopía electrónica y son: la estructura de CatSper de ratón (55) y SLO1 de humano (91) (Figura 3). Ambas secuencias cuentan con un nivel de identidad con su homólogo igual o superior al 50 o 45%, respectivamente. De esta forma, es posible generar modelos por homología de estos canales para su uso en estudios *in silico* (92).

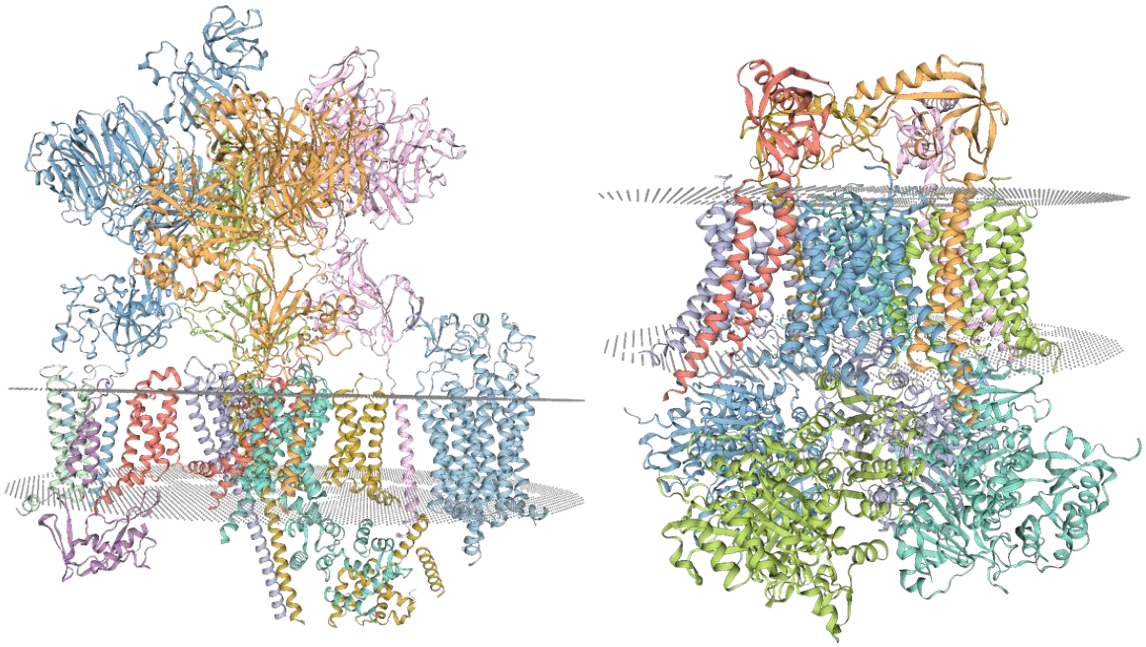

Figura 3. Vista lateral de las estructuras de CatSper de ratón (izquierda) y SLO1 de humano (derecha). Ambas estructuras fueron determinadas experimentalmente mediante crio-microscopía electrónica. CatSper (55), SLO1 (91).

En general, combinar el enfoque computacional con ensayos funcionales resulta en una estrategia atractiva para la caracterización e identificación de potenciales anticonceptivos masculinos. De esta forma, resulta necesario analizar de forma *in silico* e *in vitro* el potencial inhibitorio de moléculas sobre los canales SLO3 y CatSper del espermatozoide humano.

III. Hipótesis

Hi: Moléculas identificadas *in silico* afectan la funcionalidad del espermatozoide humano.

Ho: Moléculas identificadas *in silico* no afectan la funcionalidad del espermatozoide humano.

IV. Objetivos

Objetivo general

Analizar de forma *in silico* e *in vitro* el potencial inhibitorio de moléculas sobre los canales SLO3 y CatSper en la funcionalidad del espermatozoide humano

Objetivos específicos

Determinar la estructura de CatSper y SLO3 mediante homología.

Obtener la estructura de las potenciales moléculas inhibidoras de los canales CatSper y SLO3.

Determinar a los ligandos candidatos en función de su puntaje de acoplamiento molecular.

Validar los resultados *in silico* mediante espectrofluorometría y microscopía.

V. Metodología

- Modelado por homología

Debido a la ausencia de estructuras resueltas de los canales de interés, se determinaron las coordenadas atómicas mediante modelado por homología. El primer paso consistió en la búsqueda e identificación de secuencias plantillas. Esto es, secuencias con estructura tridimensional resuelta y un porcentaje de identidad mayor al 25% con la secuencia objetivo. Para esto, se realizó un BLAST proteína-proteína (BLASTp) empleando las secuencias de las subunidades alfa del canal CatSper (UNIPROTKB Q8NEC5, Q96P56, Q86XQ3 y Q7RTX7) y SLO3 de humano (UNIPROTKB A8MYU2).

Encontrada la mejor plantilla, su secuencia se utilizó para modelar la estructura tridimensional de los canales empleando el servidor SWISS-MODEL. A continuación, los modelos generados se alinearon con la estructura de SLO1 de humano y CatSper de ratón mediante el programa de Discovery Studio 2016. De esta forma, se alineó cada subunidad para formar el homotetrámero de SLO3 y el heterotetrámero de CatSper.

A continuación, los modelos se protonaron a pH de 7.4 utilizando el módulo proteinprepare de playmolecule y addH de Chimera 1.15, para las estructuras de SLO3 y CatSper, respectivamente.

Una vez ajustado el estado de protonación de los canales, los modelos se minimizaron *in vacuo* empleando el campo de fuerza para proteínas de Amber ff14SB durante 1000 pasos del algoritmo de descenso rápido en el programa de Chimera 1.15. Una vez hecho esto, se evaluó la calidad de estos mediante gráficos de Ramachandran empleando Molprobity v. 4.4, QMEAN del servidor de SWISS-MODEL y su alineación estructural empleando al servidor de RaptorX.

- Selección de los potenciales ligandos

Comprobada la calidad de los modelos, se obtuvieron las estructuras de los potenciales ligandos. Para SLO3 se empleó la base de datos UniprotKM. En este caso, se restringió la búsqueda a proteínas con reportes de alterar la actividad de canales de potasio tipo slo y sus estructuras se obtuvieron de la base de estructuras de proteínas Alphafold (93). Por su parte, para el canal CatSper, se emplearon las estructuras de 2315 fármacos aprobados por la FDA disponibles en el servidor de DrugRep.

- Acoplamiento y dinámica molecular

Para la realización del acoplamiento molecular entre toxinas y SLO3, se restringió el acoplamiento a la porción extracelular del canal de SLO3. En este paso, se identificó la hidrofobicidad del canal mediante la escala de Kyte-Doolittle empleada en el programa de Discovery Studio 2016. Así mismo, se redujo el sistema de SLO3,

eliminando el dominio sensor de calcio y el de voltaje (73). En cambio, para el acoplamiento molecular entre los fármacos y CatSper, se restringió el acoplamiento a la región del poro del canal.

A continuación, para validar los modelos, se realizaron acoplamientos moleculares empleando inhibidores conocidos de los canales. Para SLO3 se utilizó a la iberiotoxina (ibtx) y se acopló mediante el servidor de HADDOCK 2.4. Así mismo, se evaluó la estabilidad del complejo SLO3-ibtx mediante simulaciones de dinámica molecular. En este caso, se empleó el servidor de CHARMM-GUI para la construcción del sistema, se minimizó la energía por el algoritmo de descenso pronunciado y se equilibró el sistema empleando el protocolo de CHARMM-GUI. Finalmente, se realizaron simulaciones de dinámica molecular en el programa Gromacs durante 100 ns y se evaluó la raíz de la desviación cuadrática media entre el complejo y la toxina.

En el caso de CatSper, se utilizó el programa de Autodock Vina para acoplar las moléculas: HC-056456, Mibefradil, ML218, RU1968, Sertralina y las primeras moléculas identificadas de las series 1, 2, 6 y 7 del estudio de Carlson y colaboradores (68). Por su parte, como controles negativos se generaron 50 moléculas señuelo por cada uno de los inhibidores de CatSper antes mencionados, empleando el programa de DUD-E. Finalmente, se utilizaron los puntajes de acoplamiento molecular obtenidos para generar una curva ROC con el fin de validar el modelo y determinar el mejor punto de corte.

- Cribado virtual

Una vez validados los modelos de los canales, se procedió al cribado virtual empleando ZDOCK 3.0.2 para SLO3 y Autodock Vina para CatSper. En el caso de SLO3, las toxinas que obtuvieron un puntaje de acoplamiento molecular igual o superior que la ibtx se consideran ligandos candidatos del canal. Por su parte, los ligandos candidatos de CatSper son aquellos fármacos que obtuvieron un puntaje de acoplamiento molecular superior al punto de corte de la curva ROC.

- Obtención de las muestras de semen

Realizado lo anterior, se procedió a la parte *in vitro* del proyecto. Para el cálculo de la muestra, se utilizó el programa GPower 3.1, asumiendo un tamaño del efecto de 0.8, alfa de una cola de 0.05 y un poder de 0.8 para un análisis de varianza de 4 grupos. Así, se reclutaron a 8 participantes masculinos con una edad de 18 a 30 años. Se excluyeron a aquellos participantes con uso de narcóticos o fármacos, con enfermedades crónico degenerativas, que reportaron enfermedades de transmisión sexual o que hubieran presentado un cuadro febril en los últimos tres meses previos. De igual forma, se eliminaron de la muestra a los participantes con parámetros de calidad del semen anormales de acuerdo a la quinta edición del manual de la OMS.

Una vez firmada la carta de consentimiento informado, se solicitó la muestra de semen con 2 a 7 días de abstinencia sexual. Las muestras de semen, obtenidas mediante masturbación, se colocaron en frascos estériles individuales. Posterior a esto, se evaluaron los parámetros de calidad del semen. Brevemente, las muestran se incubaron por 30 minutos a condiciones estándar para que ocurra el proceso de licuefacción. Después, se tomaron alícuotas para determinar: el porcentaje de motilidad, la morfología mediante tinciones eosina-hematoxilina, la concentración espermática en una cámara Makler y el pH de la muestra.

- Preparación de la muestra de espermatozoides

Posteriormente, las muestras se prepararon mediante la técnica de nado hacia arriba en un tubo de ensayo inclinado a 45°. Para esto, 500 µL de la muestra se incubaron con 500 µL de medio Ham's F10 suplementado con 5 mg/mL de BSA a condiciones estándar durante 1 h. Se tomaron 400 µL de la fase superior y se ajustó la concentración de espermatozoides a $1x10^7$ células/ml con medio Ham's F10 suplementado. Finalmente, las muestras se incubaron por 3 horas más para capacitar a los espermatozoides de la muestra.

- Evaluación del efecto de los ligandos candidatos en la funcionalidad del espermatozoide humano

Para valorar la inhibición de la actividad de CatSper, se evaluó los cambios en la fluorescencia del marcador $DiSC_3(5)$ mediante espectrofluorometría antes y

después de remover el Na^+ extracelular por EGTA. De forma similar, para valorar la inhibición de la actividad del canal de SLO3, se evaluó la fluorescencia del marcador $DiSC_3(5)$ mediante espectrofluorometría (Figura 4).

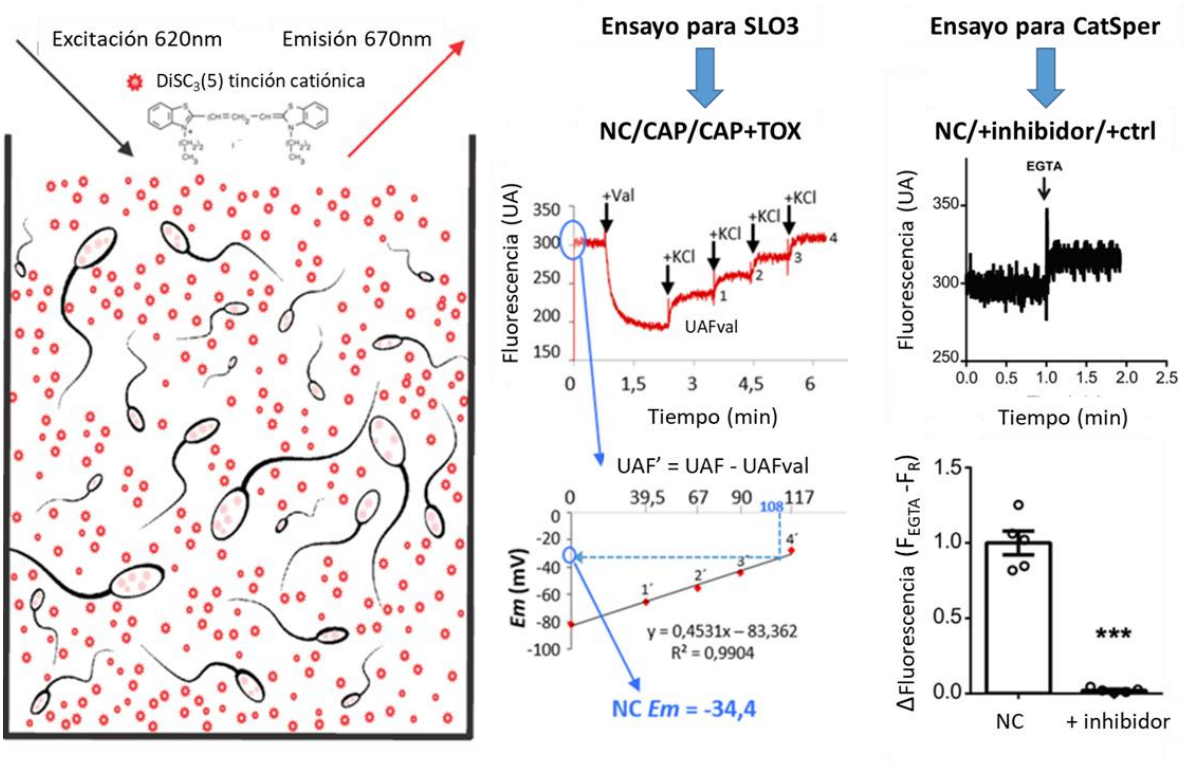

Figura 4. Ensayos funcionales para identificar inhibidores de la actividad de CatSper y SLO3. Para SLO3, se determinará el potencial de membrana en espermatozoides capacitados y no capacitados, mediante la calibración con el ionóforo de valinomicina. Por su parte, para CatSper se analizará la fluorescencia normalizada (fluorescencia posterior a la administración de EGTA – fluorescencia promedio de un minuto previo a la administración de EGTA) en condiciones no capacitantes, en presencia o ausencia de los potenciales inhibidores de CatSper. Tomado y modificado de Ritagliati *et al*., 2018 (94) y de Luque *et al*., 2023 (71).

Así mismo, se evaluaron los porcentajes de hiperactivación de espermatozoides capacitados en presencia o ausencia de los ligandos candidatos. Para esto, la hiperactivación se evaluó mediante el plugin de OpenCASA del programa ImageJ, definiendo a los espermatozoides hiperactivados como aquellos con: velocidad

curvilínea (> 150 µm/s), linearidad (< 50%) y desplazamiento lateral de la cabeza (≥ 3.5 µm).

Finalmente, se evaluó el porcentaje de espermatozoides reaccionados de forma espontánea e inducidos por progesterona. Para esto, se teñiron con la lectina *Pisum sativum* acoplada a isotiocianato de fluoresceína (FITC-PSA) durante 30 minutos. Finalmente, después de lavar el exceso de FITC-PSA, se evaluó la región acrosomal mediante microscopia de fluorescencia.

- Análisis estadístico

Para el análisis estadístico, se evaluó la distribución de los datos mediante la prueba de normalidad de Shapiro-Wilk para la selección de pruebas paramétricas y no paramétricas. En el caso de comparaciones múltiples, se empleó la prueba de ANOVA o Kruskall-Wallis, seguido de la prueba post-hoc de Tukey o Dunn, respectivamente.

VI. Resultados y Discusión

Journal of Molecular Modeling (2025) 31:155
https://doi.org/10.1007/s00894-025-06379-8

ORIGINAL PAPER

Differential molecular interactions between iberiotoxin and human SLO3 and SLO1 potassium channels

Jorge Arturo Torres Juárez[1] · Ana Gabriela Hernández Puga[1] · Ana Alicia Sánchez Tusie[1]

Received: 26 September 2024 / Accepted: 28 April 2025

Abstract

Context SLO1and SLO3 are similar voltage-gated K + channels. However, SLO3 expression is sperm specific and plays an important role in the hyperpolarization of the sperm membrane potential that is crucial for sperm fertilization. This makes SLO3 an excellent molecular target for the development of male contraceptives, and computational methods can facilitate structural insights for this drug development. Here, we evaluated the differential molecular interactions between the human SLO3 (hSLO3) and SLO1 (hSLO1) potassium channels and iberiotoxin (IbTX), a toxin that selectively blocks SLO channels. To do this, molecular docking and dynamics were implemented on the channel-toxin complexes to help elucidate atomistic details of their interaction and binding energy. Our analysis found that IbTX has a similar binding energy to both channels but interacts in a distinct manner with them. Particularly, Trp14 and Arg25 residues of IbTX diverges in their interaction with the residues Val283 and Asn260 residues of hSLO3 and the corresponding residues Tyr359 and Ala336 of hSLO1. Knowledge of key residues in the molecular interface of IbTX blockage can help guide and hasten non-hormonal contraceptive development. Our results encourage the use of toxins as scaffolds for specific SLO3 blockers.

Methods Atomistic molecular dynamics were implemented on the channel-toxin complexes. To generate the complexes, IbTX was docked to the channels using HADDOCK. CHARMM-GUI was used to generate simulation systems. GROMACS v2023.1 was used to run the simulations for 500 ns in an NPT ensemble at 297.26 K employing the CHARMM36 force field. Binding energy was evaluated by molecular mechanics generalized born surface area (MM/GBSA) with gmxMMPBGBSA.py.

Keywords SLO3 · Male contraceptive · Molecular dynamics · Binding energy

Introduction

The steady increase in human population and the accompanying high unintended pregnancy rates pose a pressing threat to public health [1]. As such, novel male contraceptive methods are urgently needed. One promising target is the potassium channel SLO3. SLO3 belongs to the SLO (Maxi-K or BK) subfamily of potassium channels, and its exclusive expression in human spermatozoa [2] carries the potential to evade side effects.

SLO3 is the principal K + channel in human sperm [2], and it has an important role during sperm capacitation, since it allows hyperpolarization of the membrane potential. This hyperpolarization has been related to hyperactivation of the flagellar beat and to the acrosome reaction, which is an exocytotic event that releases enzymes that allow sperm to fertilize the egg [3]. Furthermore, knockout models of SLO3 [4] and men with missense and splice-site variant mutations in the *slo3* gene [5, 6] are infertile. Nevertheless, with the wide tissular expression of SLO1, paralogue of SLO3, potential inhibitors must have a higher preference to SLO3 if they are to reach the market. This is particularly relevant, considering that SLO1 modulates excitatory signals in both neuro and endocrine cells [7].

SLO1 and SLO3 have seven transmembrane domains with an extracellular N-terminus. Both have similar cores formed by homo-tetramers of alfa-subunits, and the opening of both channels is regulated by the voltage sensor. Both channels present long cytoplasmic structures; however, the tail of SLO3 is activated by intracellular alkalinization, while SLO1 tail is activated by intracellular calcium [8, 9].

✉ Ana Alicia Sánchez Tusie
ana.sanchez@uaq.mx

[1] Faculty of Medicine, Autonomous University of Querétaro, Santiago de Querétaro, Mexico

Published online: 13 May 2025

Recently, Lyon et al. [3] found an inhibitor (VU0546110) with higher specificity for hSLO3 than hSLO1, which pharmacologically blocked hSLO3 and diminished the fertility potential of human spermatozoa. Even more, they demonstrated that the toxin IbTX blocks both channels, with a higher potency to hSLO1. Nonetheless, depending on the physical screening of available compounds, it highly limits the research to chance alone and makes it expensive and laborious [10].

A valuable and complementary tool in drug discovery is computational techniques [11]. These have been used in male contraceptive research to find new inhibitors of key molecular targets [12, 13] and provide molecular details of their interaction [14]. Molecular dynamics have been implemented to evaluate toxins and ion channel interaction [15] and tune toxin selectivity [16, 17]. For these reasons, in order to provide structural insights for the rationalization and further design of specific hSLO3 inhibitors, we employed computational techniques to examine the IbTX/hSLO3 and IbTX/hSLO1 complexes and compared their differential molecular interactions.

Methods

Homology modeling

Due to the absence of the experimental three-dimensional structure of hSLO3, we obtained the coordinates of the channel using homology modeling. The amino acid sequence of the channel was recovered from UniProtKb (A8MYU2) [18], and BLAST protein–protein research [19] was carried out in the Protein Data Bank [20]. BLAST results located the structure of hSLO1. Using the closed conformation structure as template (RSCB 6 V35), the theoretical model of hSLO3 was generated using the SWISS-MODEL server [21]. Structural alignment to the corresponding hSLO1 structure in Discovery Studio 2016 was implemented to obtain the homotetramer structure of hSLO3. Up next, the hSLO3 model was protonated to a pH of 7.4 using the protein prepare module of the play molecule server [22]. Once the protonation state was adjusted, the model was minimized in vacuo using the Amber ff14SB forcefield with 1000 steps of steepest descents in Chimera 1.15 [23]. Finally, to evaluate the structural quality of the model, structural alignment, local geometry, and Ramachandran plot analysis were carried in the SWISS-MODEL [24] and Raptor X servers [25].

For IbTX, the structure was recovered from the database of proteins Alphafold (UNIPROT P24663) [26]. In the case of hSLO1, the experimental structure in closed conformation (RSCB 6 V35) was employed, following the same steps of hSLO3 for model refinement.

Molecular docking

Once the models were obtained, restrained-based molecular docking was implemented between the channel structures and IbTX using HADDOCK 2.4 [27]. For this, docking was restricted to the extracellular region of the channels, defined as the hydrophilic portion identified on a Kyte-Doolittle scale in Discovery Studio 2016. In the case of IbTX, the toxin residues K27 and R34 were defined as active residues, based on experimental implication [28, 29]. For docking parameters, sampling, scoring and analysis parameters default values were used. From the top cluster, the docking pose with the smallest HADDOCK score was selected. Interactions of the complexes were then evaluated with Ligplot + Dimplot [30].

Molecular dynamics

Initial structures for molecular dynamics were chosen according to the Z score and HADDOCK score of the complexes. The systems were prepared using CHARMM-GUI membrane builder [31]. Briefly, the complexes were embedded in a POPC bilayer of 88 and 90 lipids in the upper and lower layers, respectively. The systems were solvated with TIP3P and neutralized with 41 and 51 sodium and chlorine ions, corresponding to a concentration of 0.15 M. All the above, was assembled in a $90 \times 90 \times 107$ Å box. Next, using GROMACS v2023.1 [32], the CHARMM36 force field was typed [33].

Long-range electrostatic interactions were handled using the Particle Mesh Ewald method, while bonds were kept rigid with the LINCS algorithm. The system was minimized using the steep descent algorithm using 5000 steps or until a maximum force of less than 1000 kj/mol/nm was obtained.

After minimization, the systems were equilibrated using the standard CHARMM-GUI protocol of six equilibration steps. Finally, the simulations were run for 500 ns in an NPT ensemble at 297.15 K and 1 atm using the v-rescale thermostat and the Parrinello-Rahman barostat.

Trajectory analysis

Trajectories were analyzed with GROMACS packages. Root mean square deviation (RMSD) between the channels and IbTX allowed us to analyze the stability of the complexes. The average number of hydrogen bonds formed between the channels was analyzed. Finally, binding energy and decomposition analysis was evaluated by MM/GBSA with gmxMMPBGBSA.py [34], employing the

frames of the whole simulation. For this, GB-OBC1 model was selected, and internal dielectric constant was set to 1 [35]. For decomposition analysis, the energy decomposition scheme was set to 1, and all other parameters were set to default.

Results and discussion

Modeling and molecular docking

BLASTp research identified the structure of hSLO1 channels in open (RSCB 6V22) and closed conformation (RSCB 6V35). These structures were experimentally determined through electron cryo-microscopy and have a resolution comparable to structures resolved through X-ray crystallography and nuclear magnetic resonance [36].

hSLO1 shares a sequence identity of 45% with the complete sequence of hSLO3 and raises up to 65% in the pore domain (Figure S1a). Given that a sequence identity over 30% is considered sufficient for the generation of theoretical models [37], we used the hSLO1 structures as a template for the generation of the homology models of hSLO3 in open and closed conformation. However, considering that IbTX has been added to spermatozoa before capacitation, which would correspond to an inactive state of SLO3, we limited further experiments to the hSLO3 model in closed conformation.

Once the homology model was determined, we evaluated its structural quality. According to the RMSD of the alignment, the generated model has a high structural similarity to its template (Figure S1b). In the case of the Ramachandran plot, 95% of amino acids were found in favorable regions, which correspond to a correct stereochemical configuration (Figure S1c). Finally, according to the QMEANbrane value of 0.84 (where one is the maximum value), the model possesses good local geometry (Figure S1d). Overall, this assessment demonstrates the high quality of our hSLO3 homology model.

The structure of IbTX was obtained from the Alphafold database. This model presents high confidence prediction levels in all its residues, and all their amino acids are located in favorable regions (Figure S2). Further supporting its use, it has been estimated that small proteins predicted through Alphafold have more or the same quality than models obtained through nuclear magnetic resonance [38].

With the quality of the three-dimensional structures confirmed, we obtained the IbTX/hSLO3 and IbTX/hSLO1 complexes with HADDOCK. We observed that K27 of the IbTX occluded the pore channel of hSLO3 coordinated by the Phe279 residues of the selective filter (Fig. 1a). This result is consistent with the binding mode of alpha-KTx toxins, where a basic residue inserts into the pore of the channel [39]. Similar results were obtained on the IbTX/hSLO1 complex (Fig. 1b). However, in contrast to the IbTX/hSLO3 complex, IbTX forms more hydrogen bonds with hSLO1. Being residues Gly356, Tyr359, and Lys361 of hSLO1 involved in multiple hydrogen bonds with IbTX, not observed in the IbTX/hSLO3 complex.

Based on the structural alignment, Gly356 and Lys361 would correspond to the conserved Gly280 and Lys285 of hSLO3, whereas Tyr359 of hSLO1 corresponds to the smaller Val283 of hSLO3. This last residue has been proposed to be important in establishing selectivity to toxins in potassium channels. Particularly, Chen and Chung [40] suggested that a change of Tyr381 to Val381 favors the preference of maurotoxin to Kv1.2 over Kv1.1 channels. In the context of the alpha-KTx 01 subfamily, charybdotoxin has a higher selectivity to Kv1.1 than Kv1.2 [40], which could indicate that a Tyr residue in this position is more beneficial than a Val residue in this subfamily of toxins. Indeed, mutagenesis analysis has shown that Y359 V reduces the affinity of IbTX to hSLO1 [41].

One possible explanation for this reduced affinity is the types of interactions in which these residues are involved. For example, Gly356, Lys361, and Tyr359 of hSLO1 form hydrogen bonds with Cys7, Trp14, Cys28, Asp24, Gly26, and Tyr36 of IbTX, whereas Cys7, Trp14, Cys28, and Tyr36 make hydrophobic contacts with hSLO3. In this way, binding of IbTX to hSLO3 appears to depend more on hydrophobic contributions and could help explained the reduced potency of IbTX to hSLO3, compared to hSLO1 [3].

Molecular dynamics

To evaluate the stability of the previous complexes and validate the binding modes, molecular dynamics simulations were carried out. CHARMM-GUI server was used to construct the systems (Fig. 2). Once the system was built, it was minimized and equilibrated using the standard CHARMM-GUI protocol. Finally, molecular dynamics simulations were run in Gromacs for 500 ns.

Both complexes remained stable after 60 ns of the simulations, according to the RMSD between complex and toxin (Fig. 3, left), with the exception of a transient increase of the RMSD of the hSLO3/IbTX complex at 400 ns due to the partial movement of a flexible loop of IbTX (Movie S1). In contrast to hSLO3, hSLO1 required lower times for stabilization, explained by the higher initial number of hydrogen bonds seen in the complexes (Fig. 3, right).

Up next, we explored the average hydrogen bond formation between the residues of the toxin seen in the docking model and the ion channels (Table S1). As expected, we saw that Val283 of hSLO3 does not form hydrogen bonds with IbTX, in contrast to Tyr359 of hSLO1. Similarly, Ser8, Trp14, Arg25, and Asp24 of IbTX forms more hydrogen

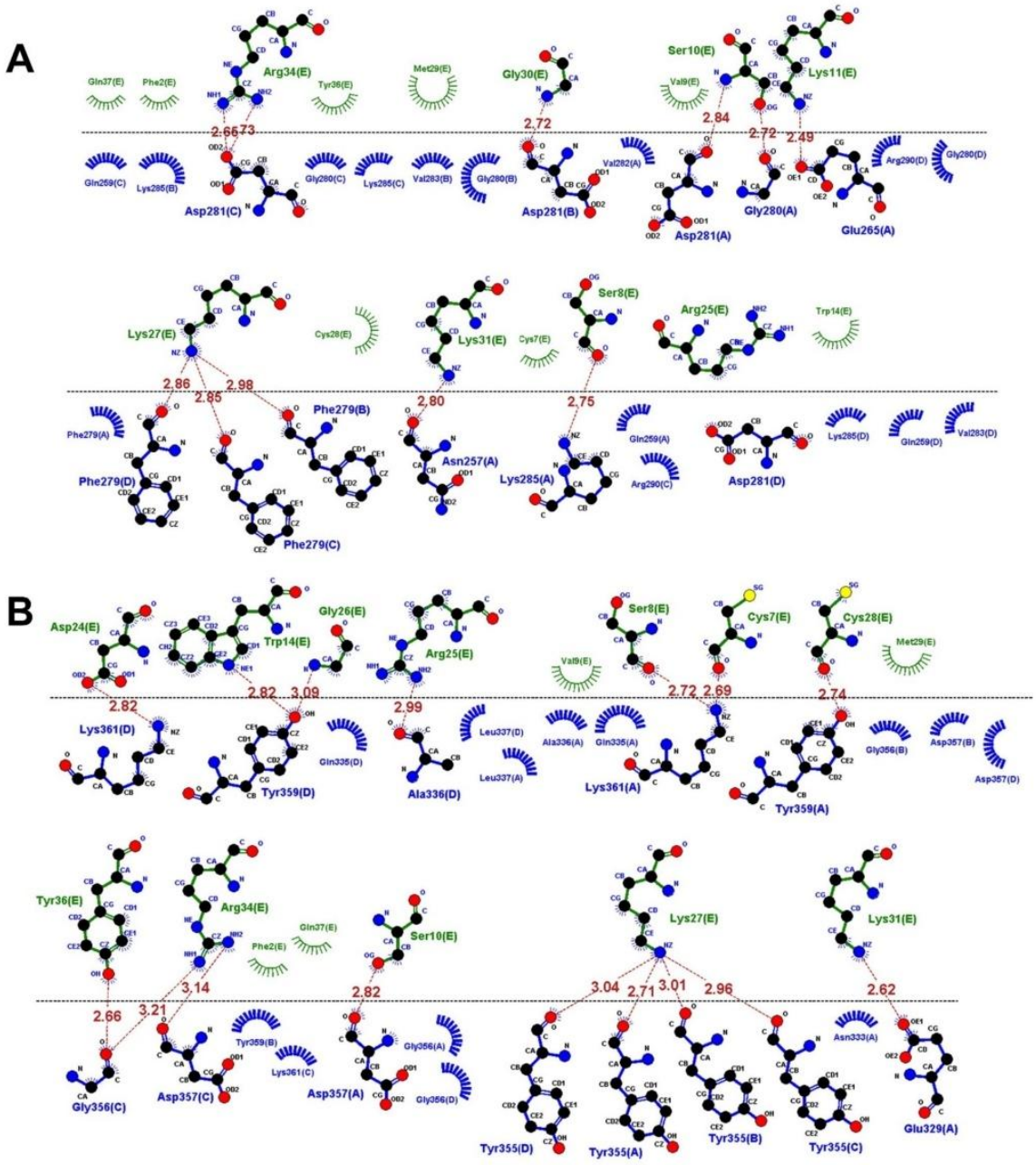

Fig. 1 Molecular interactions between IbTX with hSLO3 (**A**) and hSLO1 channels (**B**) in the binding mode obtained by docking. Amino acids of IbTX (above) are separated from the channel residues (below) by the middle-dotted lines. Hydrogen bonds are represented as dotted lines, while hydrophobic contacts are represented as radial spikes

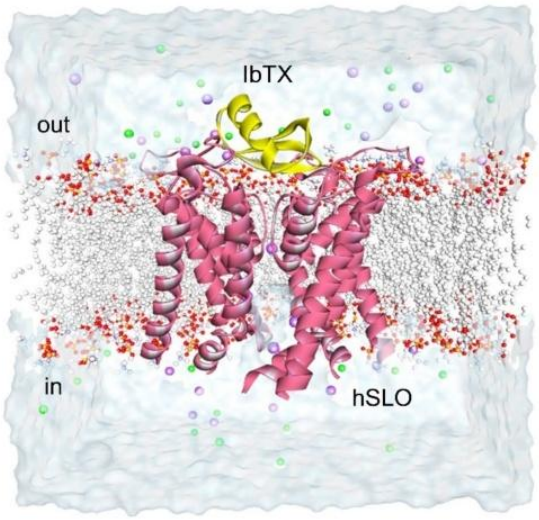

Fig. 2 Representative image of the molecular dynamics systems. hSLO channels are embedded in a POPC bilayer, solvated with TIP3P and neutralized with sodium and chlorine ions. IbTX is shown occluding the pore of the channel

bonds with hSLO1 than with hSLO3. However, in contrast to the binding mode obtained by docking, Ser10, Gly30, and Lys31 made more hydrogen bonds with hSLO1 than with hSLO3.

Binding energy

To further explore these differences, we analyzed the binding energy of the complexes applying MM/GBSA. We observed a higher binding energy in the complex of IbTX/hSLO1, compared to IbTX/hSLO3 (− 55.72 vs. − 18.23 kcal/mol), as expected of their potency difference [3]. Though we did not explore the potential influence of the LRRC52 auxiliary subunit and more rigorous studies of free energy calculation are required to validate the binding energies obtained, finding similar binding energy differences supported by the literature prompt us to analyze the binding energy contribution of each amino acid in the toxin-channel complexes.

Here, we saw that Trp14, Arg25, Arg34, and Tyr36 made a higher contribution in the binding energy of IbTX/hSLO1, compared to IbTX/hSLO3 (Fig. 4a). To explore the potential value of modifying these residues, we subtracted the side chain contribution from the total contribution of each amino acid to the binding energy. We found that the side chain contribution of Trp14 and Arg25 is important to hSLO1 but not to hSLO3, which is in agreement with the hydrogen bond exploration and the docking model (Table S1; Fig. 1).

With this, we proposed that Tyr359 of hSLO1 interacts with Trp14 via hydrogen bond formation, whereas Val283 of hSLO3 is limited to hydrophobic interactions. Similarly, Ala336 of hSLO1 makes a hydrogen bond with Arg25, in contrast to the hydrophobic interaction between Asn260 of hSLO3 and Arg25 of IbTX (Fig. 4b; Table S2; Figure S3). In this way, our model suggests that modifying Trp14 and Arg25 of IbTX should reduce its affinity to hSLO1, with minimal alterations in its interaction with hSLO3. Indeed, mutagenesis analysis shows that Trp14 and Arg25 of the homologous toxin, charybdotoxin, are crucial for the binding of BK channels [42].

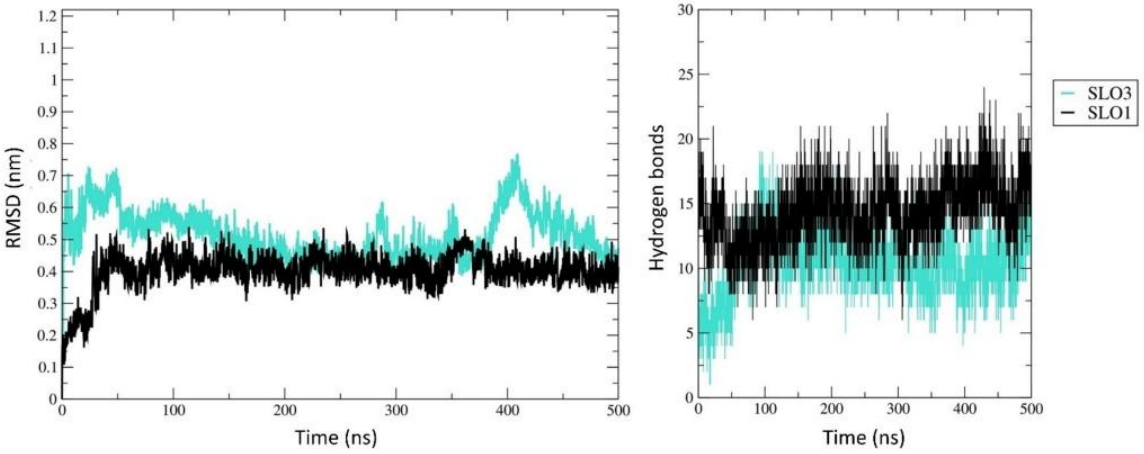

Fig. 3 Trajectory analysis of the IbTX/hSLO3 and IbTX/hSLO1 complexes. **A** RMSD of the complexes and the toxin. **B** Number of hydrogen bonds formed during the time of simulation between SLO1 and SLO3 with IbTX

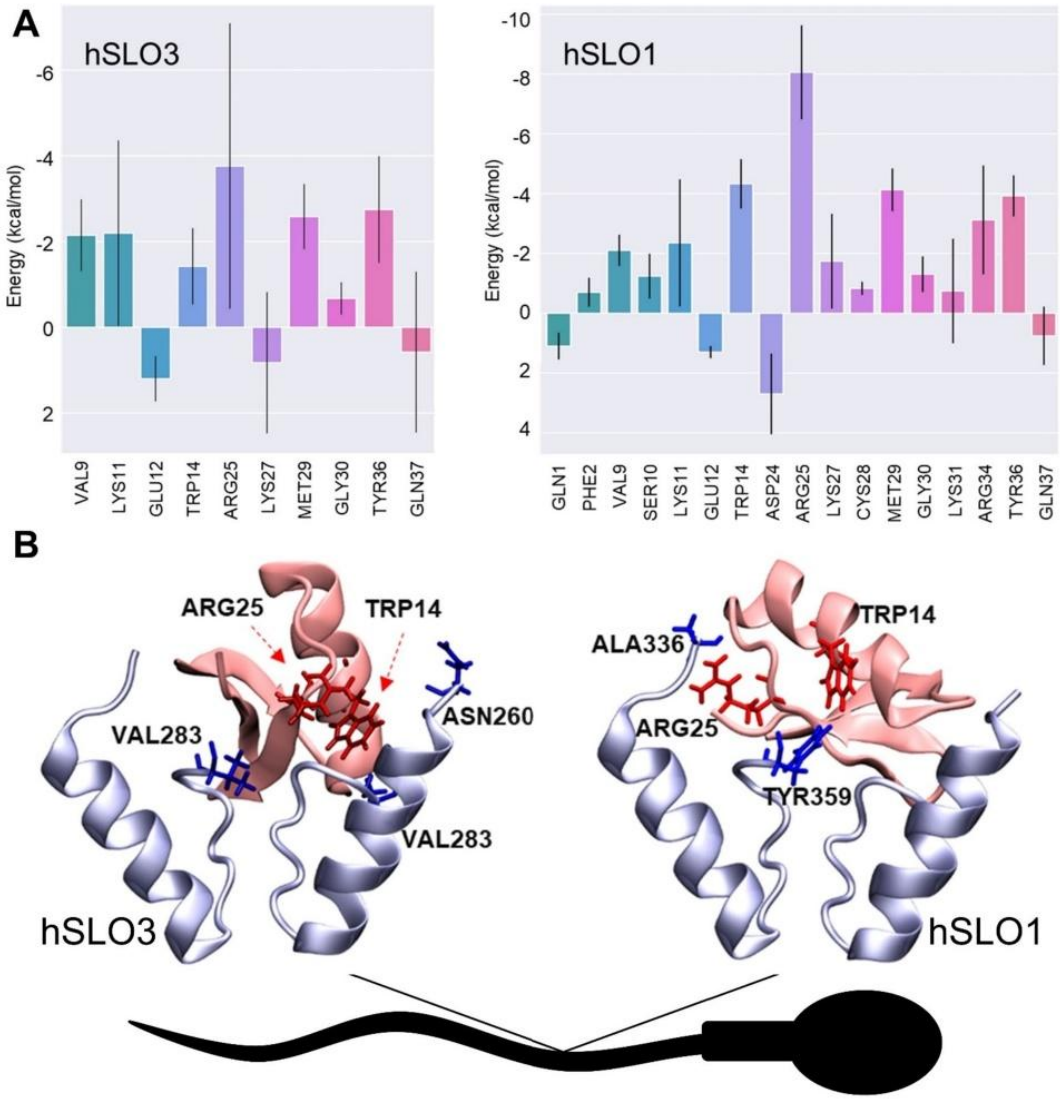

Fig. 4 Energy contribution and overall model of the blockage of hSLO3 and hSLO1 by IbTX. **A** Residue decomposition for IbTX/hSLO3 and IbTX/hSLO1 complexes. Negative energy values reflect active residues of IbTX in the blockage of the SLO channels. **B** Schematic representation of the proposed differential binding mode of IbTX. In the absence of a Tyr residue at position 283 in hSLO3, Val283 mediates the hydrophobic interaction with Trp14 of IbTX. Similarly, Asn260 of hSLO3 is limited to hydrophobic interactions with Arg25, in contrast to the hydrogen bond between Ala336 of hSLO1 and Arg25

Conclusions

In this work, the differential molecular interactions between IbTX and the hSLO3 and hSLO1 channels were explored using molecular dynamics. The simulations show that Ala336 of the turret region and Tyr359 of the selective filter of hSLO1 confer a greater affinity to IbTX when compared to Val283 and Asn260 of hSLO3. Potential partners mediating this interaction are Trp14 and Arg25 of IbTX, making them candidates for the alteration of IbTX specificity. Overall, our results support the role of IbTX as an hSLO3 blocker, identifying key residues in the binding mode of the complexes with the hope to speed the much-needed development of novel male contraceptives.

Supplementary Information The online version contains supplementary material available at https://doi.org/10.1007/s00894-025-06379-8.

Acknowledgements This work was supported by a grant from Autonomous University of Querétaro (UAQ) (FOPER-2022-FME02922). J.A.T.J. is a PhD student from the Doctorado en Ciencias en Biomedicina (UAQ), under a fellowship from CONAHCYT.

Author contribution J.A.T.J. perfomed the research and drafted the manuscript. A.G.H.P. adviced in the use of the homology program and analysis of the data. A.A.S.T. revised the manuscript critically and supervised the project. All authors reviewed the manuscript and contributed to the final version.

Data availability Data is provided within the supplementary information files.

Data and software availability Electronic supplementary material is available alongside the manuscript.

Declarations

Competing interests The authors declare no competing interests.

References

1. Nickels L, Yan W (2024) Nonhormonal male contraceptive development— strategies for progress. https://doi.org/10.1124/pharmrev.122.000787. American Society for Pharmacology and Experimental Therapy (ASPET)
2. Brenker C et al (2014) The Ca2+-activated K+ current of human sperm is mediated by Slo3. Elife 2014(3):1–19. https://doi.org/10.7554/eLife.01438
3. Lyon M et al (2023) A selective inhibitor of the sper-specific potassium channel SLO3 impairs human sperm function. Proc Natl Acad Sci 120(4):pp. https://doi.org/10.1073/pnas
4. Santi CM et al (2010) The SLO3 sperm-specific potassium channel plays a vital role in male fertility. FEBS Lett 584(5):1041–1046. https://doi.org/10.1016/j.febslet.2010.02.005
5. Lv M et al (2022) Homozygous mutation in SLO3 leads to severe asthenoteratozoospermia due to acrosome hypoplasia and mitochondrial sheath malformations. Reprod Biol Endocrinol 20(1). https://doi.org/10.1186/s12958-021-00880-4
6. Liu R et al (2022) Bi-allelic variants in KCNU1 cause impaired acrosome reactions and male infertility. Hum Reprod 37(7):1394–1405. https://doi.org/10.1093/humrep/deac102
7. Contreras GF et al (2013) A BK (Slo1) channel journey from molecule to physiology. Taylor and Francis Inc. https://doi.org/10.4161/chan.26242
8. Schreiber M, Wei A, Yuan A, Gaut J, Saito M, Salkoff L (1998) Slo3, a novel pH-sensitive K+ channel from mammalian spermatocytes. J Biol Chem 273(6):3509–3516. https://doi.org/10.1074/jbc.273.6.3509
9. Hou S, Xu R, Heinemann SH, Hoshi T (2008) Reciprocal regulation of the Ca2+ and H+ sensitivity in the SLO1 BK channel conferred by the RCK1 domain. Nat Struct Mol Biol 15(4):403–410. https://doi.org/10.1038/nsmb.1398
10. DiMasi JA, Grabowski HG, Hansen RW (2016) Innovation in the pharmaceutical industry: new estimates of R&D costs. J Health Econ 47:20–33. https://doi.org/10.1016/j.jhealeco.2016.01.012
11. De Vivo M, Masetti M, Bottegoni G, Cavalli A (2016) Role of molecular dynamics and related methods in drug discovery. Am Chem Soc. https://doi.org/10.1021/acs.jmedchem.5b01684
12. Ayoub AM et al (2017) BET bromodomain inhibitors with one-step synthesis discovered from virtual screen. J Med Chem 60(12):4805–4817. https://doi.org/10.1021/acs.jmedchem.6b01336
13. Kyzer J et al (2023) Investigation of selective retinoic acid receptor alpha antagonist ER-50891 and related analogs for male contraception. Arch Pharm e2300031. https://doi.org/10.1002/ardp.202300031
14. Rand M, Silva E, Hamil K (2016) Non-hormonal male contraception: a review and development of an Eppin based contraceptive. Pharmacol Ther 157(3):105–111. https://doi.org/10.1053/j.gastro.2016.08.014.CagY
15. Yuan S, Gao B, Zhu S (2017) Molecular dynamics simulation reveals specific interaction sites between scorpion toxins and Kv1.2 channel: implications for design of highly selective drugs. Toxins (Basel) 9(11). https://doi.org/10.3390/toxins9110354
16. Yin SJ et al (2008) Different residues in channel turret determining the selectivity of ADWX-1 inhibitor peptide between Kv1.1 and Kvl. 3 channels. J Proteome Res 7(11):4890–4897. https://doi.org/10.1021/pr800494a
17. Gigolaev AM et al (2020) Tuning scorpion toxin selectivity: switching from KV1.1 to KV1.3. Front Pharmacol 11. https://doi.org/10.3389/fphar.2020.01010
18. Bateman A et al (2017) UniProt: the universal protein knowledgebase. Nucleic Acids Res 45(D1):D158–D169. https://doi.org/10.1093/nar/gkw1099
19. Altschul SF et al (1990) Basic Local Alignment Search Tool. J Mol Biol 215(3):403–410. https://doi.org/10.1016/S0022-2836(05)80360-2
20. Velankar S, Burley SK, Kurisu G, Hoch JC, Markley JL (2021) The protein data bank archive. In: Owens R (ed) Structural proteomics, 3rd edn. Humana Press, pp 3–21. https://doi.org/10.1007/978-1-0716-1406-8_1. ch. 1
21. Waterhouse A et al (2018) SWISS-MODEL: homology modelling of protein structures and complexes. Nucleic Acids Res 46(W1):W296–W303. https://doi.org/10.1093/nar/gky427
22. Martínez-Rosell G, Giorgino T, De Fabritiis G (2017) PlayMolecule ProteinPrepare: a web application for protein preparation for molecular dynamics simulations. J Chem Inf Model 57(7):1511–1516. https://doi.org/10.1021/acs.jcim.7b00190
23. Pettersen EF et al (2004) UCSF Chimera - a visualization system for exploratory research and analysis. J Comput Chem 25(13):1605–1612. https://doi.org/10.1002/jcc.20084
24. Studer G, Biasini M, Schwede T (2014) Assessing the local structural quality of transmembrane protein models using statistical potentials (QMEANBrane). In: Bioinformatics. Oxford University Press. https://doi.org/10.1093/bioinformatics/btu457
25. Källberg M et al (2012) Template-based protein structure modeling using the RaptorX web server. Nat Protoc 7(8):1511–1522. https://doi.org/10.1038/nprot.2012.085
26. Varadi M (2022) AlphaFold protein structure database: massively expanding the structural coverage of protein-sequence space with high-accuracy models. Nucleic Acids Res 50(D1):D439–D444. https://doi.org/10.1093/nar/gkab1061
27. Van Zundert GCP et al (2016) The HADDOCK2.2 Web Server: user-friendly integrative modeling of biomolecular complexes. J Mol Biol 428(4):720–725. https://doi.org/10.1016/j.jmb.2015.09.014
28. Giangiacomo K (1999) Electrostatic mutations in Iberiotoxin as a unique tool for probing the electrostatic structure of the Maxi-K Channel Outer Vestibule †. https://doi.org/10.1021/bi982040
29. Gao YD, Garcia ML (2003) Interaction of agitoxin2, charybdotoxin, and iberiotoxin with potassium channels: selectivity between voltage-gated and Maxi-K channels. Proteins Struct Funct Genet 52(2):146–154. https://doi.org/10.1002/prot.10341

30. Laskowski RA, Swindells MB (2011) LigPlot+: multiple ligand-protein interaction diagrams for drug discovery. J Chem Inf Model 51(10):2778–2786. https://doi.org/10.1021/ci200227u
31. Wu EL et al (2014) CHARMM-GUI membrane builder toward realistic biological membrane simulations. John Wiley and Sons Inc. https://doi.org/10.1002/jcc.23702
32. Páll S et al (2020) Heterogeneous parallelization and acceleration of molecular dynamics simulations in GROMACS. J Chem Phys 153(13). https://doi.org/10.1063/5.0018516
33. Huang J, Mackerell AD (2013) CHARMM36 all-atom additive protein force field: validation based on comparison to NMR data. J Comput Chem 34(25):2135–2145. https://doi.org/10.1002/jcc.23354
34. Valdés-Tresanco MS, Valdés-Tresanco ME, Valiente PA, Moreno E (2021) gmx_MMPBSA: a new tool to perform end-state free energy calculations with GROMACS. J Chem Theory Comput 17(10):6281–6291. https://doi.org/10.1021/acs.jctc.1c00645
35. Chen F et al (2016) Assessing the performance of the MM/PBSA and MM/GBSA methods. 6. Capability to predict protein-protein binding free energies and re-rank binding poses generated by protein-protein docking. Phys Chem Chem Phys 18(32):22129–22139. https://doi.org/10.1039/c6cp03670h
36. Cassidy K, Himes BA, Luthey-Schulten Z, Zhang P (2018) CryoEM-based hybrid modeling approaches for structure determination. Curr Opin Microbiol 43:14–23. https://doi.org/10.1016/j.mib.2017.10.002
37. Haddad Y, Adam V, Heger Z (2020) Ten quick tips for homology modeling of high-resolution protein 3D structures. PLoS Comput Biol 16(4):1–19. https://doi.org/10.1371/journal.pcbi.1007449
38. Tejero R, Huang YJ, Ramelot TA, Montelione GT (2022) AlphaFold models of small proteins rival the accuracy of solution NMR structures. Front Mol Biosci 9(June):1–18. https://doi.org/10.3389/fmolb.2022.877000
39. Chen R, Chung S-H (2015) Computational studies of venom peptides targeting potassium channels. Toxins (Basel) 7(12):5194–5211
40. Chen R, Chung SH (2012) Structural basis of the selective block of Kv1.2 by Maurotoxin from computer simulations. PLoS One 7(10). https://doi.org/10.1371/journal.pone.0047253
41. Giangiacomo KM, Becker J, Garsky C, Schmalhofer W, Garcia ML, Mullmann TJ (2008) Novel α-KTx sites in the BK channel and comparative sequence analysis reveal distinguishing features of the BK and KV channel outer pore. Cell Biochem Biophys 52(1):47–58. https://doi.org/10.1007/s12013-008-9026-3
42. Stampe P, Kolmakova-Partensky L, Miller C (1994) Intimations of K+ channel structure from a complete functional map of the molecular surface of charybdotoxin? Biochemistry 33(2):443-50

International Journal of
Molecular Sciences

MDPI

Article

Pimozide Inhibits CatSper Activity, Impairs Hyperactivation and the Acrosome Reaction in Human Spermatozoa

Jorge Arturo Torres Juárez [1], Ana Gabriela Hernández Puga [1], Esperanza Mata Martínez [2], Claudia Lydia Treviño Santa Cruz [3] and Ana Alicia Sánchez Tusie [1,*]

[1] Centro de Investigación Biomédica Avanzada, Facultad de Medicina, Universidad Autónoma de Querétaro (UAQ), Santiago de Querétaro 76010, Mexico; jtorres65@alumnos.uaq.mx (J.A.T.J.); ana.gabriela.hernandez@uaq.mx (A.G.H.P.)
[2] Departamento de Biología Celular y Desarrollo, Instituto de Fisiología Celular, Universidad Nacional Autónoma de México (UNAM), Ciudad de México 04510, Mexico; espemmtz@gmail.com
[3] Departamento de Genética del Desarrollo y Fisiología Molecular, Instituto de Biotecnología (IBT), Universidad Nacional Autónoma de México (UNAM), Cuernavaca 62210, Mexico; claudia.trevino@ibt.unam.mx
* Correspondence: ana.sanchez@uaq.mx

Abstract

Health, social, and ethical considerations highlight the need for new male contraceptives. Pimozide is an FDA approved drug known to block T-type calcium channels and which shares structural similarities with mibefradil, a proven antagonist of the CatSper channel. In this study, we examined the effect of pimozide on CatSper, a key target for non-hormonal male contraception. Molecular docking and molecular dynamics simulations were carried out to assess how pimozide binds within the channel pore, and binding energies were estimated using MM-GBSA. To determine its impact on sperm function, we evaluated hyperactivation, the acrosome reaction, and CatSper activity. Our computational analyses indicate that pimozide functions as a pore blocker of the CatSper channel. Experimental findings further support this, showing that pimozide inhibits CatSper activity, and impairs hyperactivation and the acrosome reaction in human spermatozoa. Overall, these results identify pimozide as a novel CatSper antagonist and propose a binding mode, offering a basis for the rational design of reversible, non-hormonal male contraceptives that target the CatSper channel.

Keywords: male contraception; CatSper; molecular dynamics; pimozide

Academic Editor: Alessandra Ferramosca

Received: 27 November 2025
Revised: 2 January 2026
Accepted: 8 January 2026
Published: date

1. Introduction

The need for novel male contraceptives arises from several concerns: the rapid growth of the global population and its environmental impact [1], the high incidence of unintended pregnancies and their negative consequences for health and socioeconomic stability [2], the limited options and drawbacks of current male contraceptives [3], and the ethical imperative to share responsibility in family planning [4].

Novel male contraceptive methods are generally classified into hormonal and non-hormonal approaches [5]. Hormonal methods have shown promise in clinical studies, but side effects have hindered their progress toward commercialization [6]. In contrast, non-hormonal strategies are considered more attractive. Mechanical approaches, such as vas

deferens blockers, have advanced to clinical trials [7], and one target-based strategy is also in testing [8]. However, the high attrition rates in drug development highlight the importance of pursuing alternative molecular targets.

The CatSper channel, a sperm-specific cation channel essential for male fertility, is an attractive non-hormonal target [9,10]. CatSper is a complex ion channel composed of at least 14 subunits, four α-subunits form its heterotetrameric pore region. CatSper plays a vital role during sperm capacitation, being the principal channel responsible for calcium influx in spermatozoa. This influx of calcium is needed for sperm to acquire hyperactivation, an asymmetric motile pattern that allows spermatozoa to navigate the viscous female reproductive tract. For CatSper, several antagonists have been reported [11–20], but structural insights remain limited, slowing drug development. To accelerate this process, drug and scaffold repurposing are valuable strategies to consider.

Here, we investigated the potential of pimozide, an antipsychotic drug approved for tics treatment in Tourette's syndrome [21] as an antagonist of CatSper. Particularly, we choose pimozide for a variety of reasons. Since pimozide is an FDA approved drug, repurposing holds the potential to hasten the development of male contraceptives. Furthermore, pimozide is structurally similar to mibefradil, a known antagonist of CatSper. Finally, since it's known that pimozide acts as a pore blocker to other calcium channels, we could evaluate in silico the pore blocking action of pimozide on the CatSper channel.

2. Results

2.1. Homology Modelling

For the determination of the three-dimensional structure of the CatSper, we employed homology modelling. For this, we used the α-subunits of the known structure of the mouse Catsper channel, which is in a presumed closed conformation due to its pore dimensions. The amino acid sequence of α-subunits of the human CatSper channel has mean 66.23% identity with the mouse CatSper channel. Since this value exceeds the minimum rule of thumb of 30%, we used the SWISS-MODEL server for the generation of the model. With respect to its structural quality, over 95% of the amino acids of the model are in favorable regions of the Ramachandran plot (Figure S1a). Furthermore, the model presents a score of 0.85 in QMEANbrane (https://swissmodel.expasy.org/qmean/, accessed on 1 January 2026), a web software specialized in quality assessment of membrane proteins (Figure S1b). Taking these results together, our model presents optimal stereochemistry and local geometry.

2.2. Molecular Docking and Molecular Dynamics

After evaluating the quality of our model, we proceeded with the docking of pimozide. Since the pore of the human Cav3.3 channel is the binding site of pimozide and mibefradil, a known antagonist of CatSper, we selected the pore of CatSper channel as the binding site. The docking score of the top pose was −10.9 kcal/mol, indicating a favorable interaction.

To evaluate the stability of pimozide on the pore of the CatSper channel, we simulated the system for 500 ns (Figure 1a). We saw that pimozide remained in the pore of the channel throughout the simulation time period (Video S1), and that after 350 ns, all the four replicas remained stable, with two of the four replicas presenting two or more transient stable conformations (Figure 1b).

https://doi.org/10.3390/xxxxx

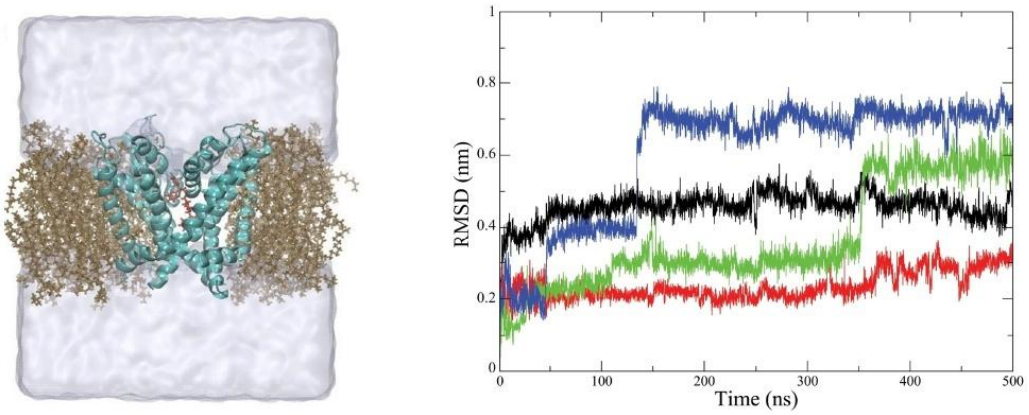

(**a**) (**b**)

Figure 1. Molecular dynamics of the CatSper-Pimozide complex. (**a**) Representation of the molecular system. The pore of the CatSper channel is shown in cyan, embedded in a POPC bilipid layer in brown. Pimozide is shown in red, occluding the pore. (**b**) RMSD of the complex during 500 ns of simulation. Each color represents a replica of the system.

To obtain the most representative binding mode, we selected the top cluster of the last 100 ns of each simulation. Hydrophobic interactions between the rings of pimozide and the subunits of CatSper appeared consistently in all replicas (Figure 2). Hydrophobic interactions are mediated by the fluorophenyl rings and the benzimidazole ring. Hydrogen bonds were formed in the piperidine ring in its amide group in three of the four replicas with an asparagine, and in the fluorine atoms in two of the four replicas (Figure S2).

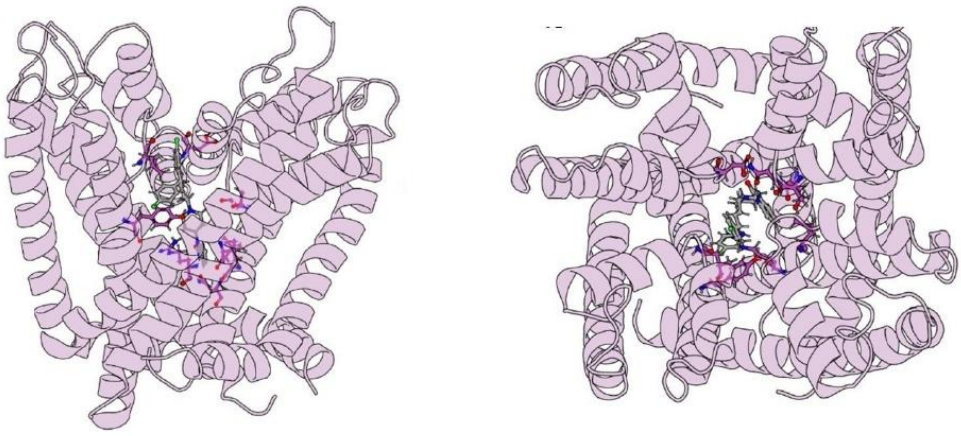

(**a**) (**b**)

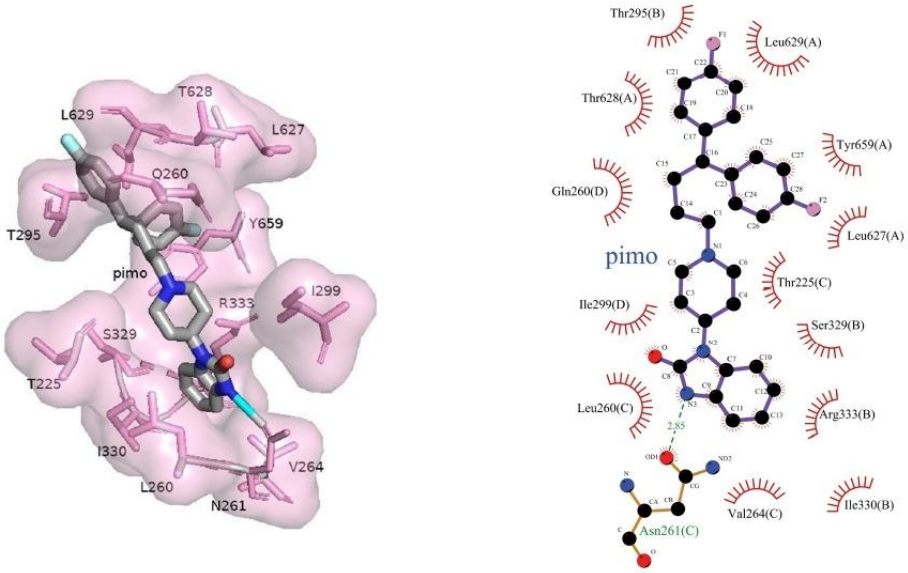

(**c**) (**d**)

Figure 2. Binding mode of the most representative cluster after 400 ns. (**a**,**b**) pimozide-CatSper side and top-down view. (**c**,**d**) binding mode of pimozide within the pore of CatSper. Pimozide interacts with CatSper mainly through hydrophobic interaction with its ring system.

Finally, to evaluate the binding affinity of pimozide, we estimated the Gibbs free energy with MM-GBSA. Here, we saw that pimozide presents a favorable binding energy (−109.856 kcal/mol, Table S1), which prompts us to evaluate its effect on human spermatozoa.

2.3. Sperm Hyperactivation

The hallmark of CatSper function is sperm hyperactivation [12]. During capacitation, sperm exhibit hyperactivated motility, a pattern dependent on calcium entry via CatSper, which facilitates movement through the viscous female reproductive tract [22]. Due to this, we asked if exposing sperm to pimozide could inhibit the acquisition of hyperactivation. For this, we choose concentrations of pimozide (0, 0.01, 0.1, 1, 10 and 100 μM), overlapping the peak serum concentration of 0.04 μM [23]. Here, we saw a reduction in hyperactivated spermatozoa exposed to increasing concentrations of pimozide. Pimozide acted in a dose-response manner on hyperactivation with an IC50 of 2.92 μM (Figure 3a).

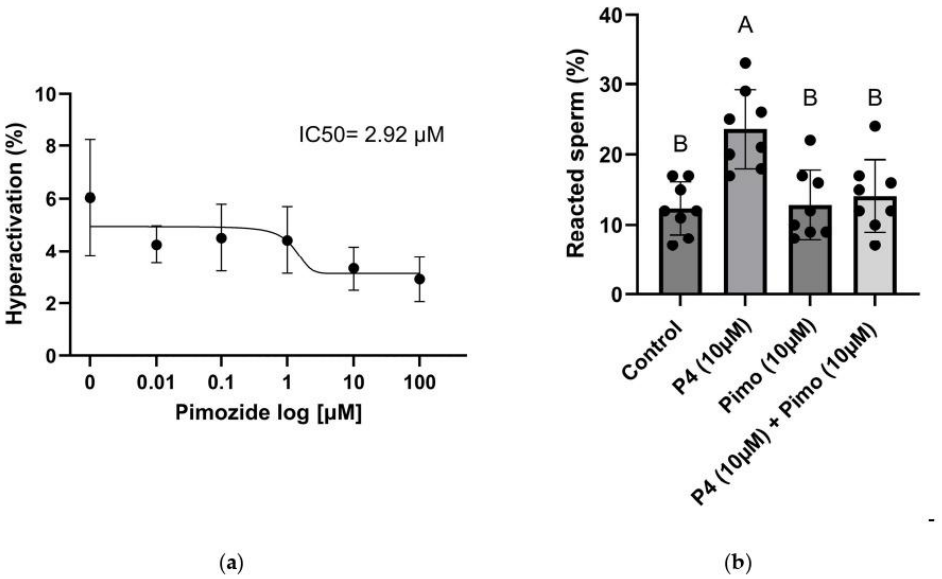

(**a**) (**b**)

Figure 3. Pimozide alters the functionality of human spermatozoa. (**a**) Human sperm were exposed to pimozide (0–100 µM) incubated for 2 h. Hyperactivation was evaluated in at least 5 different fields with OpenCASA. (**b**) After 4 h of capacitation with or without pimozide 10 µM (Pimo), spermatozoa were exposed to progesterone (P4) or DMSO (control). Results are expressed as mean ± SEM. Different letters indicate statistical differences, n = 8.

2.4. Acrosome Reaction

Another key function of sperm for human fertilization is the acrosome reaction (AR). This reaction is an exocytotic process that depends on calcium and allows sperm to bind to the ovum [24]. Though the involvement of CatSper in the AR is debated [9,25], this reaction can be induced with progesterone, an agonist of CatSper and a physiological inductor of the AR [15,16,24]. To compare the potency of pimozide with other antagonists of CatSper, we evaluated its effect using a concentration of 10 µM pimozide. Here, we saw that the number of reacted spermatozoa was significantly higher in the group exposed to progesterone than in the control group. In contrast, spermatozoa exposed to pimozide maintained the same levels of reacted sperm as the control group, even in the presence of progesterone (Figure 3b).

2.5. CatSper Activity

While the detrimental effect of pimozide on functions dependent on calcium entry to sperm is suggestive of its action on CatSper, there is a need to employ validated assays of the activity of CatSper [26]. For this, we measured with fluorimetry the changes in the membrane potential of a population of spermatozoa after calcium chelation in the presence or absence of pimozide. In the absence of extracellular calcium, an influx of sodium mediated by CatSper depolarizes the sperm membrane. We saw that sperm exposed to pimozide in non-capacitated conditions respond significantly less to the chelation stimulus (Figure 4b).

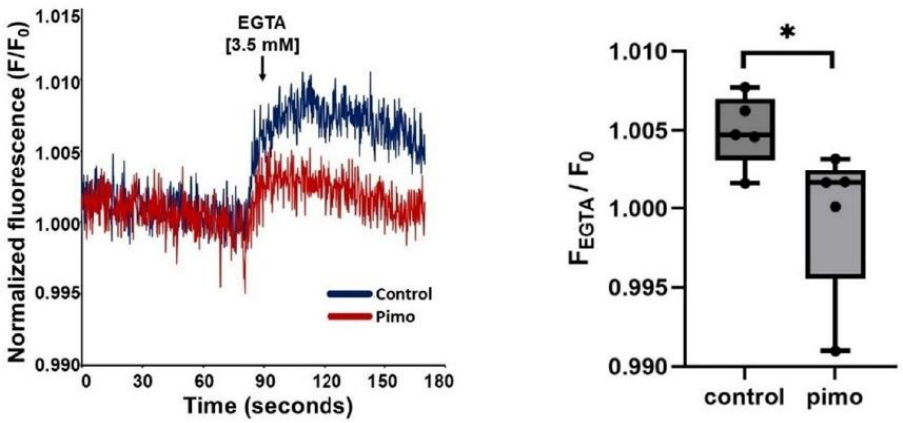

(**a**) (**b**)

Figure 4. Pimozide inhibits the activity of CatSper in non-capacitating conditions. After 5 min of basal DISC3(5) fluorescence recording, 3.5 mM of EGTA was administered to the cuvette. (**a**) Representative traces of the CatSper activity assay in non-capacitated sperm. (**b**) CatSper activity in the presence or absence of 10 μM pimozide, in non-capacitated sperm, n = 5. * $p < 0.05$.

3. Discussion

Despite the growing demand for male contraceptives, no new options have been approved. To provide a framework for the characterization of novel antagonists of CatSper, we examined with computational and experimental approaches the potential of pimozide as a pore blocker of the CatSper channel.

Molecular docking and dynamics simulations revealed favorable interactions between pimozide and the CatSper pore. The docking scores, stability of the complex, and binding free energy rescoring with MM-GBSA indicate strong binding. The predicted binding mode involves hydrophobic interactions and hydrogen bonds. This aligns with the known binding of pimozide to the human Cav3.3 channel at the fenestration site between the selectivity filter and the intracellular gate and shares the formation of a hydrogen bond between an asparagine and the benzimidazole group [27]. Interestingly, while the fluorophenyl groups of pimozide in Cav3.3 are oriented toward the intracellular gate, our model positions them near the selectivity filter, suggesting potential avenues for selectivity optimization. This is worth exploring considering the IC50 of pimozide on Cav3.3 vs CatSper (0.77 vs. 2.92 μM) [27]. Enhancing shape complementarity between ligand and receptor, for example, by introducing hydrophobic moieties to occupy the binding cavity, is a proven strategy to improve affinity and reduce off-target effects [28]. Indeed, structure-activity relationship studies have applied this approach to pimozide, successfully reducing its affinity for dopamine receptors [29], reinforcing its potential as a scaffold for male contraceptive development. However, future studies, using patch-clamp electrophysiology and experimental structure determination techniques, are needed to validate the pore blocking action of pimozide and the proposed binding mode.

To explore our computational findings, we assessed the effects of pimozide on human sperm function. Pimozide induced a dose-dependent decrease in the percentage of hyperactivated sperm, consistent with previous reports on other CatSper antagonists, including RU1968 [18], mibefradil, ML218, medroxyprogesterone acetate, levonorgestrel, aldosterone [11], HC-056456 [12], and NNC55-0396 [30]. With respect to the IC50 of pimozide, this was comparable to the IC50 of other antagonists of CatSper (Table 1).

Table 1. IC50 comparisons between known CatSper antagonists and pimozide.

Compound	IC50 (μM)	Method of Determination	Reference
RU1968F1	0.4	Patch-clamp	[18]
Tetrahydrocannabinol	1.88	Fluorimetry	[20]
Cannabidiol	2.47	Fluorimetry	[20]
Pimozide	2.92	Hyperactivation	This study
HC-056456	3	Fluorimetry	[12]
RU1968F1	3.1	Fluorimetry	[18]
ML218	5	Fluorimetry	[11]
Medroxiprogesterone	6.1	Fluorimetry	[11]
Sertraline	4.61–16.19	Fluorimetry	[19]
Mibefradil	6.18–18	Fluorimetry	[16]

The AR also depends on calcium entry [24]. Pimozide has been previously shown to reduce the AR induced with solubilized zona pellucida in human sperm [31]. Here, we looked at the effect of pimozide in the AR induced with progesterone and observed similar results. Since the zona pellucida elicits the AR by stimulating CatSper via a different mechanism than progesterone [32], our results argue in favor of a direct action of pimozide on CatSper.

Other antagonists of CatSper reported to reduce the percentage of AR induced by progesterone are: RU1968 [18], HC-056456 [12], mibefradil [25], and sertraline [19]. Similarly to others [18], pimozide did not increase the spontaneous AR (sAR) percentage, sAR is the acrosome reaction that occurs without the presence of any inducer, like progesterone that can be used as a positive control. However, some studies have reported an increase in the sAR in the presence of known inhibitors in capacitated [20,33] and non-capacitated sperm [34].

To evaluate the activity of CatSper in a validated assay, we measured the changes in the membrane potential before and after chelating extracellular calcium in the presence or absence of pimozide. We saw that pimozide was capable of reducing the response of this chelating stimulus. Future studies could explore ligand binding to the channel in an open state and assess different incubation times. Moreover, our study was limited by not modeling additional CatSper subunits, restricting the evaluation of other potential binding sites. Finally, due to the reported cardiotoxicity of pimozide and its known ability to block T-type calcium channels and dopamine receptors, development of male contraceptives based on this scaffold must carefully consider selectivity profiles or possible side effects.

4. Materials and Methods

4.1. Homology Modeling

The structure of the human CatSper channel was modeled using the SWISS-MODEL server (https://swissmodel.expasy.org, accessed on 1 January 2026) [35]. The α-subunits from the Catspermasome structure (RCSB 7EEB) served as templates [36], and structural alignment was performed to reconstruct the heterotetrameric, pore-forming region of the channel. The model was protonated at pH 7.4 using the AddH module in Chimera v1.15 [37]. Model quality was assessed via Ramachandran plots, while local geometry was evaluated using the QMEANbrane web server [38].

4.2. Molecular Docking

The structure of pimozide was recovered from the Drug Bank database [39] and was energy-minimized in Avogadro V1.2.0 with the MMFF94 force field and the steepest descent algorithm [40]. Open Babel V3.1.1 was used to convert to the PDBQT format [41]. Next, the CatSper pore was selected as the docking site. A grid box of 26 × 26 × 26 Å covering the pore was used, and docking was conducted with AutoDock Vina (version 1.2.7) [42]. The highest-scoring pose of the pimozide-CatSper complex was selected for molecular dynamics simulations.

4.3. Molecular Dynamics

The complex was embedded in a POPC membrane, solvated with TIP3P water, and neutralized with Na^+ and Cl^- ions at 0.15 M using CHARMM-GUI (https://www.charmm-gui.org, accessed on 1 January 2026) [43]. Simulations were run in GROMACS 2023.5 [44] with the CHARMM36f force field [45], and pimozide topology was assigned via CGenFF [46]. Electrostatics were treated with the Particle Mesh Ewald method, and all bonds were constrained with LINCS. Energy minimization was performed using the steepest descent algorithm for 5000 steps or until the maximum force fell below 1000 $kJ \cdot mol^{-1} \cdot nm^{-1}$. The system was equilibrated according to the six-step CHARMM-GUI protocol, followed by four 500 ns production simulations in the NPT ensemble at 310.15 K and 1 atm using the v-rescale thermostat and Parrinello-Rahman barostat.

4.4. Trajectory Analysis and Binding Free Energy

Root mean square deviation (RMSD) was calculated with GROMACS tools. The relative binding free energy was estimated using gmx_MMGBPBSA (version 1.6.4) [47], analyzing all frames from the last 100 ns of each replica at 310.15 K and 0.15 M ionic strength with the GBneck (igb7) model. The mean structure of the top cluster from the last 100 ns was selected to represent a plausible binding mode. Molecular interactions were analyzed using Ligplot+ v2.2.9, PyMOL v3.1.6.1 and the Protein Imager server (https://3dproteinimaging.com/protein-imager, accessed on 1 January 2026) [48–50].

4.5. Semen Sample Collection

For the in vitro portion of the study, ethical approval from the Ethical Committee of the Faculty of Medicine, Autonomous University of Queretaro (protocol code BIOM-013/2024-6 and date of approval 28 June 2024) was obtained. Next, 8 male participants with at least 2 days of sexual abstinence and normal semen parameters according to the WHO manual 5th edition were recruited, excluding participants with known sexually transmitted infections, chronic diseases, use of illicit substances or under pharmacological treatment. After written informed consent, semen samples were requested. According to WHO guidelines, a normal semen analysis typically shows a volume of at least 1.5 milliliters, a sperm concentration of 15 million sperm per milliliter or more, at least 40% motility, and a morphology with at least 4% of sperm having a normal shape. For this, human sperm concentration was measured with a Makler chamber. Semen volume was determined with a serological pipette. Morphology was analyzed with the Diff-Quik stain following the WHO 5th edition strict criteria. Motility was measured by placing 10 μL of the semen sample in a slide with a coverslip of 22 mm by 22 mm, categorizing sperm movement in progressive motility, non-progressive motility and immotility.

4.6. Sperm Hyperactivation

Semen samples were liquefied and processed using the swim-up method. Aliquots of 500 μL semen were layered with 500 μL Ham's F-10 medium (ThermoFisher Gibco catalog number: 11550043, Waltham, MA, USA) in Falcon tubes, inclined at 45°, and

incubated at 37 °C with 5% CO_2 for 1 h. The upper fraction was collected and adjusted to 10 × 10^6 sperm/mL. Samples were split into six groups exposed to varying concentrations of pimozide (0–100 μM) in a medium containing 5 mg/mL bovine serum albumin for 3 h. Motility was recorded in five fields per sample at 10× magnification (60 fps, 2048 × 1536 pixels), and hyperactivation was determined with OpenCASA based on a lateral head displacement (ALH) ≥ 3.5 μm, mean curvilinear velocity (VLC) > 150 μm/s, and a linearity (LIN) < 50%.

4.7. Acrosome Reaction

After swim-up, sperm were capacitated for 4 h with or without 10 μM pimozide, then treated with 10 μM progesterone or 0.1% DMSO for 30 min. Samples were centrifuged, resuspended in cold methanol, smeared, air-dried, and stained with FITC-PSA. At least 100 spermatozoa per sample were analyzed under fluorescence microscopy (498/517 nm).

4.8. CatSper Activity

Membrane potential changes in response to EGTA (F_{EGTA}) were measured in sperm adjusted to 5–10 × 10^6/mL and pretreated with 10 μM pimozide before DISC3(5) loading to a final concentration of 1 μM. 3.5 mM of EGTA was added after 5 min of basal fluorescence (F_0), with fluorescence being recorded at 620/670 nm at 37 °C. $F_{EGTA/F0}$ ratios were used to quantify CatSper activity [26].

4.9. Statistical Analysis

The distribution of the variables was evaluated with the Shapiro-Wilk test. Group comparisons were performed using paired Student's *t*-test for the CatSper Activity dataset, and repeated measures ANOVA followed by Tukey HSD test for the reacted sperm dataset. Three parameter Hill equation was fitted to estimate the half maximal inhibitory concentration (IC50). Data are presented as mean ± standard error, with $p < 0.05$ set for statistical differences. GraphPad Prism 10.2.0 software was used for all statistical analysis.

5. Conclusions

Overall, we have characterized in silico and in vitro, the non-hormonal contraceptive potential of pimozide. Our results suggest that pimozide can potentially function as a scaffold for the generation of male contraceptives targeting the complex CatSper channel, though repurposing pimozide as a CatSper antagonist is contingent on in vivo data.

Supplementary Materials: The following supporting information can be downloaded at: https://www.mdpi.com/article/doi/s1.

Author Contributions: Conceptualization, J.A.T.J. and A.A.S.T.; methodology, J.A.T.J., A.G.H.P., E.M.M., C.L.T.S.C. and A.A.S.T.; formal analysis, J.A.T.J. and A.A.S.T.; investigation, J.A.T.J.; writing—original draft preparation, J.A.T.J. and A.A.S.T.; writing—review and editing, J.A.T.J., A.G.H.P., E.M.M., C.L.T.S.C. and A.A.S.T.; supervision, A.A.S.T.; project administration, A.A.S.T.; funding acquisition, C.L.T.S.C. and A.A.S.T. All authors have read and agreed to the published version of the manuscript.

Funding: This research was funded by CONAHCYT, grant number CBF2023-2024-2680.

Institutional Review Board Statement: This study was conducted in accordance with the Declaration of Helsinki and approved by the Ethics Committee of the Faculty of Medicine, Autonomous University of Queretaro (protocol code BIOM-013/2024-6 and date of approval 28 June 2024).

Informed Consent Statement: Informed consent was obtained from all subjects involved in the study.

Data Availability Statement: The raw data supporting the conclusions of this article will be made available by the authors upon request.

Acknowledgments: J.A.T.J. is a student from the Doctorado en Ciencias en Biomedicina (UAQ), under a fellowship from CONAHCYT (926929). We are thankful to Paulina Torres Rodríguez for technical assistance in the laboratory.

Conflicts of Interest: The authors declare no conflicts of interest.

Abbreviations

The following abbreviations are used in this manuscript:

RMSD	Root mean square deviation
EGTA	Ethylene glycol tetraacetic acid
DMSO	dimethyl sulfoxide
MM	Molecular mechanics
GBSA	General Born Surface Area
RCSB PDB	Research Collaboratory for Structural Bioinformatics Protein Data Bank
POPC	1-palmitoyl-2-oleoyl-sn-glycero-3-phosphocholine
FITC-PSA	Fluorescein isothiocyanate-labeled *Pisum sativum agglutinin*

References

1. Tal, A. The Environmental Impacts of Overpopulation. *Encyclopedia* **2025**, *5*, 45. https://doi.org/10.3390/encyclopedia5020045.
2. Bearak, J.; Popinchalk, A.; Alkema, L.; Sedgh, G. Global, regional, and subregional trends in unintended pregnancy and its outcomes from 1990 to 2014: Estimates from a Bayesian hierarchical model. *Lancet Glob. Health* **2018**, *6*, e380–e389. https://doi.org/10.1016/S2214-109X(18)30029-9.
3. Abbe, C.; Page, S.; Thirumalai, A. Male contraception. *Encycl. Reprod.* **2018**, *93*, 478–485. https://doi.org/10.1016/B978-0-12-801238-3.64620-2.
4. Campelia, G.D.; Adashi, E.Y.; Amory, J.K. Shared risk and shared responsibility: The ethics of male contraceptives. *Andrology* **2024**, *12*, 1605–1609. https://doi.org/10.1111/andr.13649.
5. Service, C.A.; Puri, D.; Hsieh, T.-C.; Patel, D. Emerging concepts in male contraception: A narrative review of novel, hormonal and non-hormonal options. *Ther. Adv. Reprod. Health* **2022**, *9*, 259–261. https://doi.org/https://doi.org/10.1177/26334941221138323.
6. Page, S.T.; Blithe, D.; Wang, C. Hormonal Male Contraception: Getting to Market. *Front. Endocrinol.* **2022**, *13*, 891589. https://doi.org/10.3389/fendo.2022.891589.
7. Sidhom, K.; Bal, D.S.; Ramjiawan, R.; Patel, P. The landscape of male contraception. *Can. Urol. Assoc. J.* **2024**, *18*, 353–359. https://doi.org/10.5489/cuaj.8728.
8. Mannowetz, N.; McCallum, S.W.; Sidhu, S.; Mena, K.H.; Ruby, E.P.; Castro-Santamaria, R.; Dodds, E.; Henderson, D.; Whitaker, G.; Wright, H.; et al. Safety and pharmacokinetics of the non-hormonal male contraceptive YCT-529. *Commun. Med.* **2025**, *5*, 279. https://doi.org/10.1038/s43856-025-01004-4.
9. Young, S.; Schiffer, C.; Brenker, C.; Strunker, T. Human fertilization in vivo and in vitro requires the CatSper channel to initiate sperm hyperactivation. *J. Clin. Investig.* **2024**, *134*, e173564. https://doi.org/10.1172/JCI173564.
10. Ren, D.; Navarro, B.; Perez, G.; Jackson, A.C.; Hsu, S.; Shi, Q.; Tilly, J.L.; Clapham, D.E. A sperm ion channel required for sperm motility and male fertility. *Nature* **2001**, *413*, 603–609. https://doi.org/10.1038/35098027.
11. Carlson, E.J.; Georg, G.I.; Hawkinson, J.E. Steroidal Antagonists of Progesterone-and Prostaglandin E 1-Induced Activation of the Cation Channel of Sperm. *Mol. Pharmacol.* **2022**, *101*, 56–67. https://doi.org/10.1124/MOLPHARM.121.000349.
12. Carlson, A.E.; Burnett, L.A.; del Camino, D.; Quill, T.A.; Hille, B.; Chong, J.A.; Moran, M.M.; Babcock, D.F. Pharmacological targeting of native CatSper channels reveals a required role in maintenance of sperm hyperactivation. *PLoS ONE* **2009**, *4*, e6844. https://doi.org/10.1371/journal.pone.0006844.

13. Carlson, E.J.; Francis, R.; Liu, Y.; Li, P.; Lyon, M.; Santi, C.M.; Hook, D.J.; Hawkinson, J.E.; Georg, G.I. Discovery and Characterization of Multiple Classes of Human CatSper Blockers. *ChemMedChem* **2022**, *17*, e202000499. https://doi.org/10.1002/cmdc.202000499. Correction in *ChemMedChem* **2022**, *17*, e202200441.
14. Mannowetz, N.; Mundt, N.; Lishko, P.V. The plant triterpenoid pristimerin inhibits calcium influx into human spermatozoa via CatSper. *Proc. Natl. Acad. Sci. USA* **2018**, *115*, E347–E348. https://doi.org/10.1073/pnas.1719673115.
15. Lishko, P.V.; Botchkina, I.L.; Kirichok, Y. Progesterone activates the principal Ca^{2+} channel of human sperm. *Nature* **2011**, *471*, 387–392. https://doi.org/10.1038/nature09767.
16. Strünker, T.; Goodwin, N.; Brenker, C.; Kashikar, N.D.; Weyand, I.; Seifert, R.; Kaupp, U.B. The CatSper channel mediates progesterone-induced Ca2+ influx in human sperm. *Nature* **2011**, *471*, 382–387. https://doi.org/10.1038/nature09769.
17. Brenker, C.; Goodwin, N.; Weyand, I.; Kashikar, N.D.; Naruse, M.; Krähling, M.; Müller, A.; Benjamin Kaupp, U.; Strünker, T. The CatSper channel: A polymodal chemosensor in human sperm. *EMBO J.* **2012**, *31*, 1654–1665. https://doi.org/10.1038/emboj.2012.30.
18. Rennhack, A.; Schiffer, C.; Brenker, C.; Fridman, D.; Nitao, E.T.; Cheng, Y.M.; Tamburrino, L.; Balbach, M.; Stölting, G.; Berger, T.K.; et al. A novel cross-species inhibitor to study the function of CatSper Ca2+ channels in sperm. *Br. J. Pharmacol.* **2018**, *175*, 3144–3161. https://doi.org/10.1111/bph.14355.
19. Rahban, R.; Rehfeld, A.; Schiffer, C.; Brenker, C.; Palme, D.L.E.; Wang, T.; Lorenz, J.; Almstrup, K.; ESkakkebaek, N.; Strünker, T.; et al. The antidepressant Sertraline inhibits CatSper Ca^{2+} channels in human sperm. *Hum. Reprod.* **2021**, *36*, 2638–2648. https://doi.org/10.1093/humrep/deab190.
20. Wehrli, L.; Altevogt, H.; Brenker, C.; Zufferey, F.; Rossier, M.F.; Strünker, T.; Nef, S.; Rahban, R. The major phyto-cannabinoids, delta-9-tetrahydrocannabinol (THC) and cannabidiol (CBD), affect the function of CatSper calcium channels in human sperm. *Hum. Reprod.* **2025**, *40*, 796–807. https://doi.org/10.1093/humrep/deaf020.
21. Pringsheim, T.; Marras, C. Pimozide for tics in Tourette's syndrome. *Cochrane Database Syst. Rev.* **2009**, *2009*, CD006996. https://doi.org/10.1002/14651858.cd006996.pub2.
22. Demott, R.P.; Suarez, S.S. Hyperactivated sperm progress in the mouse oviduct. *Biol. Reprod.* **1992**, *46*, 779–785. https://doi.org/10.1095/biolreprod46.5.779.
23. Shaw, V.; Srivastava, S.; Srivastava, S.K. Repurposing antipsychotics of the diphenylbutylpiperidine class for cancer therapy. *Semin. Cancer Biol.* **2021**, *68*, 75–83. https://doi.org/10.1016/j.semcancer.2019.10.007.
24. Kirkman-Brown, J.C.; Punt, E.L.; Barratt, C.L.R.; Publicover, S.J. Zona pellucida and progesterone-induced Ca2+ signaling and acrosome reaction in human spermatozoa. *J. Androl.* **2002**, *23*, 306–315. https://doi.org/10.1002/j.1939-4640.2002.tb02232.x.
25. Tamburrino, L.; Marchiani, S.; Minetti, F.; Forti, G.; Muratori, M.; Baldi, E. The CatSper calcium channel in human sperm: Relation with motility and involvement in progesterone-induced acrosome reaction. *Hum. Reprod.* **2014**, *29*, 418–428. https://doi.org/10.1093/humrep/det454.
26. Luque, G.M.; Schiavi-Ehrenhaus, L.J.; Jabloñski, M.; Balestrini, P.A.; Novero, A.G.; Torres, N.I.; Osycka-Salut, C.E.; Darszon, A.; Krapf, D.; Buffone, M.G. High-throughput screening method for discovering CatSper inhibitors using membrane depolarization caused by external calcium chelation and fluorescent cell barcoding. *Front. Cell Dev. Biol.* **2023**, *11*, 1010306. https://doi.org/10.3389/fcell.2023.1010306.
27. He, L.; Yu, Z.; Geng, Z.; Huang, Z.; Zhang, C.; Dong, Y.; Gao, Y.; Wang, Y.; Chen, Q.; Sun, L.; et al. Structure, gating, and pharmacology of human CaV3.3 channel. *Nat. Commun.* **2022**, *13*, 2084. https://doi.org/10.1038/s41467-022-29728-0.
28. Kawasaki, Y.; Freire, E. Finding a better path to drug selectivity. *Drug Discov. Today* **2011**, *16*, 985–990. https://doi.org/10.1016/j.drudis.2011.07.010.
29. Kasanami, Y.; Ishikawa, C.; Kino, T.; Chonan, M.; Toyooka, N.; Takashima, Y.; Iba, Y.; Sekiguchi, F.; Tsubota, M.; Ohkubo, T.; et al. Discovery of pimozide derivatives as novel T-type calcium channel inhibitors with little binding affinity to dopamine D2 receptors for treatment of somatic and visceral pain. *Eur. J. Med. Chem.* **2022**, *243*, 114716. https://doi.org/10.1016/j.ejmech.2022.114716.
30. Alasmari, W.; Costello, S.; Correia, J.; Oxenham, S.K.; Morris, J.; Fernandes, L.; Ramalho-Santos, J.; Kirkman-Brown, J.; Michelangeli, F.; Publicover, S.; et al. Ca^{2+} signals generated by CatSper and Ca^{2+} stores regulate different behaviors in human sperm. *J. Biol. Chem.* **2013**, *288*, 6248–6258. https://doi.org/10.1074/jbc.m112.439356.
31. Bhandari, B.; Bansal, P.; Talwar, P.; Gupta, S.K. Delineation of downstream signalling components during acro-some reaction mediated by heat solubilized human zona pellucida. *Reprod. Biol. Endocrinol.* **2010**, *8*, 7. https://doi.org/10.1186/1477-7827-8-7.

32. Balbach, M.; Hamzeh, H.; Jikeli, J.F.; Brenker, C.; Schiffer, C.; Hansen, J.N.; Neugebauer, P.; Trötschel, C.; Jovine, L.; Han, L.; et al. Molecular Mechanism Underlying the Action of Zona-pellucida Glycoproteins on Mouse Sperm. *Front. Cell Dev. Biol.* **2020**, *8*, 572735. https://doi.org/10.3389/fcell.2020.572735.
33. Wehrli, L.; Galdadas, I.; Voirol, L.; Smieško, M.; Cambet, Y.; Jaquet, V.; Guerrier, S.; Gervasio, F.L.; Nef, S.; Rahban, R. The action of physiological and synthetic steroids on the calcium channel CatSper in human sperm. *Front. Cell Dev. Biol.* **2023**, *11*, 1221578. https://doi.org/10.3389/fcell.2023.1221578.
34. Chávez, J.C.; De La Vega-Beltrán, J.L.; José, O.; Torres, P.; Nishigaki, T.; Treviño, C.L.; Darszon, A. Acrosomal al-kalization triggers Ca 2+ release and acrosome reaction in mammalian spermatozoa. *J. Cell. Physiol.* **2018**, *233*, 4735–4747. https://doi.org/10.1002/jcp.26262.
35. Waterhouse, A.; Bertoni, M.; Bienert, S.; Studer, G.; Tauriello, G.; Gumienny, R.; Heer, F.T.; De Beer, T.A.P.; Rempfer, C.; Bordoli, L.; et al. SWISS-MODEL: Homology modelling of protein structures and complexes. *Nucleic Acids Res.* **2018**, *46*, W296–W303. https://doi.org/10.1093/nar/gky427.
36. Lin, S.; Ke, M.; Zhang, Y.; Yan, Z.; Wu, J. Structure of a mammalian sperm cation channel complex. *Nature* **2021**, *595*, 746–750. https://doi.org/10.1038/s41586-021-03742-6.
37. Pettersen, E.F.; Goddard, T.D.; Huang, C.C.; Couch, G.S.; Greenblatt, D.M.; Meng, E.C.; Ferrin, T.E. UCSF Chimera—A visualization system for exploratory research and analysis. *J. Comput. Chem.* **2004**, *25*, 1605–1612. https://doi.org/10.1002/jcc.20084.
38. Studer, G.; Biasini, M.; Schwede, T. Assessing the local structural quality of transmembrane protein models using statistical potentials (QMEANBrane). *Bioinformatics* **2014**, *30*, i505–i511. https://doi.org/10.1093/bioinformatics/btu457.
39. Knox, C.; Wilson, M.; Klinger, C.M.; Franklin, M.; Oler, E.; Wilson, A.; Pon, A.; Cox, J.; Chin, N.E.; AStrawbridge, S.; et al. DrugBank 6.0: The DrugBank Knowledgebase for 2024. *Nucleic Acids Res.* **2024**, *52*, D1265–D1275. https://doi.org/10.1093/nar/gkad976.
40. Hanwell, M.D.; Curtis, D.E.; Lonie, D.C.; Vandermeersch, T.; Zurek, E.; Hutchison, G.R. SOFTWARE Open Access Avogadro: An advanced semantic chemical editor, visualization, and analysis platform. *J. Cheminform.* **2012**, *4*, 17. https://doi.org/10.1186/1758-2946-4-17.
41. O'Boyle, N.M.; Banck, M.; James, C.A.; Morley, C.; Vandermeersch, T.; Hutchison, G.R. Open babel: An open chemical toolbox. *J. Cheminform.* **2011**, *3*, 33. https://doi.org/10.1186/1758-2946-3-33.
42. Eberhardt, J.; Santos-Martins, D.; Tillack, A.F.; Forli, S. AutoDock Vina 1.2.0: New Docking Methods, Expanded Force Field, and Python Bindings. *J. Chem. Inf. Model.* **2021**, *61*, 3891–3898. https://doi.org/10.1021/acs.jcim.1c00203.
43. Wu, E.L.; Cheng, X.; Jo, S.; Rui, H.; Song, K.C.; Dávila-Contreras, E.M.; Qi, Y.; Lee, J.; Monje-Galvan, V.; Venable, R.M.; et al. CHARMM-GUI membrane builder toward realistic biological membrane simulations. *J. Comput. Chem.* **2014**, *35*, 1997–2004. https://doi.org/10.1002/jcc.23702.
44. Páll, S.; Zhmurov, A.; Bauer, P.; Abraham, M.; Lundborg, M.; Gray, A.; Hess, B.; Lindahl, E. Heterogeneous paral-lelization and acceleration of molecular dynamics simulations in GROMACS. *J. Chem. Phys.* **2020**, *153*, 134110. https://doi.org/10.1063/5.0018516.
45. Huang, J.; Mackerell, A.D., Jr. CHARMM36 all-atom additive protein force field: Validation based on comparison to NMRdata. *J. Comput. Chem.* **2013**, *34*, 2135–2145. https://doi.org/10.1002/jcc.23354.
46. Vanommeslaeghe, K.; Hatcher, E.; Acharya, C.; Kundu, S.; Zhong, S.; Shim, J.; Darian, E.; Guvench, O.; Lopes, P.; Vorobyov, I.; et al. CHARMM general force field: A force field for drug-like molecules compatible with the CHARMM all-atom additive biological force fields. *J. Comput. Chem.* **2010**, *31*, 671–690. https://doi.org/10.1002/jcc.21367.
47. Valdés-Tresanco, M.S.; Valdés-Tresanco, M.E.; Valiente, P.A.; Moreno, E. gmx_MMPBSA: A New Tool to Perform End-State Free Energy Calculations with GROMACS. *J. Chem. Theory Comput.* **2021**, *17*, 6281–6291. https://doi.org/10.1021/acs.jctc.1c00645.
48. Laskowski, R.A.; Swindells, M.B. LigPlot+: Multiple ligand-protein interaction diagrams for drug discovery. *J. Chem. Inf. Model.* **2011**, *51*, 2778–2786. https://doi.org/10.1021/ci200227u.
49. Tomasello, G.; Armenia, I.; Molla, G. The Protein Imager: A full-featured online molecular viewer interface with server-side HQ-rendering capabilities. *Bioinformatics* **2020**, *36*, 2909–2911. https://doi.org/10.1093/bioinformatics/btaa009.
50. Janson, G.; Paiardini, A. PyMod 3: A complete suite for structural bioinformatics in PyMOL. *Bioinformatics* **2021**, *37*, 1471–1472. https://doi.org/10.1093/bioinformatics/btaa849.

VII. Conclusiones

Los modelos teóricos de los canales de CatSper y SLO3 de humano permitieron identificar potenciales moléculas antagonistas de los canales y proponer modos de unión. De estas, se caracterizó *in vitro* el efecto de pimozida sobre espermatozoides de humano, mostrando que es capaz de afectar negativamente funciones que dependen del correcto funcionamiento de CatSper.

VIII. Bibliografía

1. Mohamed EAEB, Hamed AF, Yousef FMA, Ahmed EA. Prevalence, determinants, and outcomes of unintended pregnancy in Sohag district, Egypt. Journal of the Egyptian Public Health Association. 2019;94(1):1–9.

2. Bearak J, Popinchalk A, Alkema L, Sedgh G. Global, regional, and subregional trends in unintended pregnancy and its outcomes from 1990 to 2014: estimates from a Bayesian hierarchical model. Lancet Glob Health [Internet]. 2018;6(4):e380–9. Available from: http://dx.doi.org/10.1016/S2214-109X(18)30029-9

3. Juárez F, Singh S, Maddow-Zimet I, Wulf D. Embarazo no planeado y aborto inducido en México. Guttmacher Institute. 2013;48.

4. Mujeres IN de las. www.gob.mx. 2021 [cited 2022 Dec 15]. Estrategia Nacional para la Prevención del Embarazo en Adolescentes. Available from: https://www.gob.mx/inmujeres/acciones-y-programas/estrategia-nacional-para-la-prevencion-del-embarazo-en-adolescentes-33454

5. INEGI. ESTADÍSTICAS A PROPÓSITO DEL DÍA MUNDIAL PARA LA PREVENCIÓN DEL EMBARAZO NO PLANIFICADO EN ADOLESCENTES (DATOS NACIONALES). 2021.

6. Bahk J, Yun SC, Kim Y mi, Khang YH. Impact of unintended pregnancy on maternal mental health: A causal analysis using follow up data of the Panel Study on Korean Children (PSKC). BMC Pregnancy Childbirth. 2015;15(1):1–12.

7. Yazdkhasti M, Pourreza A, Pirak A, Abdi F. Unintended pregnancy and its adverse social and economic consequences on health system: A narrative review article. Iran J Public Health. 2015;44(1):12–21.

8. Klima CS. Unintended pregnancy consequences and solutions for a worldwide problem. J Nurse Midwifery. 1998;43(6):483–91.

9. Abbe C, Page S, Thirumalai A. Male contraception. Encyclopedia of Reproduction. 2018;93:478–85.

10. United Nations - Department of Economic and Social Affairs. Contraceptive Use by Method 2019. Contraception Use by Method 2019. 2019;25.

11. Thirumalai A, Amory JK. Emerging approaches to male contraception. Fertil Steril. 2021;115(6):1369–76.

12. Reynolds-Wright JJ, Cameron NJ, Anderson RA. Will Men Use Novel Male Contraceptive Methods and Will Women Trust Them? A Systematic Review. J Sex Res. 2021;58(7):838–49.

13. Glasier R, Anakwe D, Everington CW, Martin Z, Van Der Spuy L, Cheng PC, et al. Would women trust their partners to use a male pill? Human Reproduction. 2000;15(3):646–9.

14. Heinemann K, Saad F, Wiesemes M, White S, Heinemann L. Attitudes toward male fertility control: Results of a multinational survey on four continents. Human Reproduction. 2005;20(2):549–56.

15. Alberts B, Johnson A, Lewis J, Morgan D, Raff M. Molecular biology of the Cell. Vol. 53. 2016. 1689–1699 p.

16. Guyton A, Hall J. Tratado de Fisiología Médica. 2011.

17. Darszon A, Nishigaki T, Beltran C, Treviño CL. Calcium channels in the development, maturation, and function of spermatozoa. Physiol Rev. 2011;91(4):1305–55.

18. Marchiani S, Tamburrino L, Benini F, Fanfani L, Dolce R, Rastrelli G, et al. Chromatin Protamination and Catsper Expression in Spermatozoa Predict Clinical Outcomes after Assisted Reproduction Programs. Sci Rep [Internet]. 2017;7(1):1–12. Available from: http://dx.doi.org/10.1038/s41598-017-15351-3

19. Sunanda P, Panda B, Dash C, Padhy RN, Routray P. An illustration of human sperm morphology and their functional ability among different group of subfertile males. Andrology. 2018;6(5):680–9.

20. Hernández-Silva G, Chirinos M. Proteins from male and female reproductive tracts involved in sperm function regulation. Zygote. 2019;27(1):36–45.

21. Orgebin-Crist MC. Studies on the Function of the Epididymis. Biolog. 1969;1:155–75.

22. Bedford JM. Effects of duct ligation on the fertilzing ability of spermatozoa from different regions of the rabbit epididymis. Journal of Experimental Zoology. 1967;166(2):271–81.

23. Seligman J, Kosower NS, Shalgi R. Effects of caput ligation on rat sperm and epididymis: Protein thiols and fertilizing ability. Biol Reprod. 1991;46(2):301–8.

24. AUSTIN CR. Observations on the penetration of the sperm in the mammalian egg. Aust J Sci Res B. 1951;4(4):581–96.

25. Chang MC. Fertilizing Capacity of Spermatozoa deposited into the Fallopian Tubes. Nature. 1951;(4277):697–9.

26. Gervasi MG, Visconti PE. Chang's meaning of capacitation: A molecular perspective. Mol Reprod Dev. 2016;83(10):860–74.

27. Davis BK. Influence of Serum Albumin on the Fertilizing Ability In Vitro of Rat Spermatozoa. Proceedings of the Society for Experimental Biology and Medicine. 1976;151(2):240–2.

28. Zeng Y, Oberdorf JA, Florman HM. pH regulation in mouse sperm: Identification of Na+-, Cl--, and HCO-3-dependent and arylaminobenzoate-dependent regulatory mechanisms and characterization of their roles in sperm capacitation. Dev Biol. 1996;173(2):510–20.

29. Visconti PE, Moore GD, Bailey JL, Leclerc P, Connors SA, Pan D, et al. Capacitation of mouse spermatozoa pathway. Regulation. 1995;1150:1139–50.

30. Zeng Y, Clark EN, Florman HM. Sperm membrane potential: Hyperpolarization during capacitation regulates zona pellucida-dependent acrosomal secretion. Vol. 171, Developmental Biology. 1995. p. 554–63.

31. López-González I, Torres-Rodríguez P, Sánchez-Carranza O, Solís-López A, Santi CM, Darszon A, et al. Membrane hyperpolarization during human sperm capacitation. Mol Hum Reprod. 2014;20(7):619–29.

32. Yanagimachi R. the Movement of Golden Hamster. J Reprod Fertil. 1970;23:193–6.

33. Demott RP, Suarez SS. Hyperactivated sperm progress in the mouse oviduct. Biol Reprod. 1992;46(5):779–85.

34. Suarez SS, Dai X. Hyperactivation enhances mouse sperm capacity for penetrating viscoelastic media. Biol Reprod. 1992;46(4):686–91.

35. Stauss CR, Votta TJ, Suarez SS. Sperm motility hyperactivation facilitates penetration of the hamster zona pellucida. Biol Reprod. 1995;53(6):1280–5.

36. Dan J. C. Studies on the Acrosome . I . Reaction to Egg-Water and Other Stimuli Author (s): J . C . Dan Published by : Marine Biological Laboratory Stable URL : http://www.jstor.org/stable/1538405 Accessed : 21-06-2016 01 : 21 UTC. Biological Bulletin. 1952;103(1):54–66.

37. Yanagimachi R, Chang MC. Fertilization of hamster eggs in vitro [38]. Nature. 1963;200(4903):281–2.

38. Page ST, Blithe D, Wang C. Hormonal Male Contraception: Getting to Market. Front Endocrinol (Lausanne). 2022;13(June):1–7.

39. Nguyen BT, Swerdloff R, Wu FCW, Wang C. Male hormonal contraception [Internet]. 2nd ed. Encyclopedia of Endocrine Diseases. Elsevier Inc.; 2018. 741–750 p. Available from: http://dx.doi.org/10.1016/B978-0-12-801238-3.95922-1

40. Long JE, Lee MS, Blithe DL. Male contraceptive development: Update on novel hormonal and nonhormonal methods. Clin Chem. 2019;65(1):153–60.

41. Service CA, Puri D, Hsieh TC, Patel D. Emerging concepts in male contraception: a narrative review of novel, hormonal and non-hormonal options. Ther Adv Reprod Health. 2022;9(6):259–61.

42. Amouroux M, Mieusset R, Desbriere R, Opinel P, Karsenty G, Paci M, et al. Are men ready to use thermal male contraception? Acceptability in two French populations: New fathers and new providers. PLoS One. 2018;13(5):1–23.

43. Balbach M, Rossetti T, Ferreira J, Ghanem L, Ritagliati C, Myers RW, et al. On-demand male contraception via acute inhibition of soluble adenylyl cyclase. Nat Commun. 2023;14(1).

44. Ren D, Navarro B, Perez G, Jackson AC, Hsu S, Shi Q, et al. A sperm ion channel required for sperm motility and male fertility. Nature. 2001;413(6856):603–9.

45. Quill TA, Ren D, Clapham DE, Garbers DL. A voltage-gated ion channel expressed specifically in spermatozoa. Proc Natl Acad Sci U S A. 2001;98(22):12527–31.

46. Jin JL, O'Doherty AM, Wang S, Zheng H, Sanders KM, Yan W. Catsper3 and Catsper4 encode two cation channel-like proteins exclusively expressed in the testis. Biol Reprod. 2005;73(6):1235–42.

47. Schreiber M, Wei A, Yuan A, Gaut J, Saito M, Salkoff L. Slo3, a novel pH-sensitive K+ channel from mammalian spermatocytes. Journal of Biological Chemistry. 1998;273(6):3509–16.

48. Santi CM, Martínez-López P, de la Vega-Beltrán JL, Butler A, Alisio A, Darszon A, et al. The SLO3 sperm-specific potassium channel plays a vital role in male fertility. FEBS Lett. 2010 Mar 5;584(5):1041–6.

49. Hildebrand MS, Avenarius MR, Fellous M, Zhang Y, Meyer NC, Auer J, et al. Genetic male infertility and mutation of CATSPER ion channels. European Journal of Human Genetics [Internet]. 2010;18(11):1178–84. Available from: http://dx.doi.org/10.1038/ejhg.2010.108

50. Liu R, Yan Z, Fan Y, Qu R, Chen B, Li B, et al. Bi-Allelic variants in KCNU1 cause impaired acrosome reactions and male infertility. Human Reproduction. 2022 Jul 1;37(7):1394–405.

51. Liu J, Xia J, Cho KH, Clapham DE, Ren D. CatSperβ, a novel transmembrane protein in the CatSper channel complex. Journal of Biological Chemistry. 2007;282(26):18945–52.

52. Wang H, Liu J, Cho KH, Ren D. A novel, single, transmembrane protein CATSPERG is associated with CATSPER1 channel protein. Biol Reprod. 2009;81(3):539–44.

53. Chung JJ, Navarro B, Krapivinsky G, Krapivinsky L, Clapham DE. A novel gene required for male fertility and functional CATSPER channel formation in spermatozoa. Nat Commun. 2011;2(1).

54. Chung JJ, Miki K, Kim D, Shim SH, Shi HF, Hwang JY, et al. Catsperς regulates the structural continuity of sperm ca2+ signaling domains and is required for normal fertility. Elife. 2017;6:1–25.

55. Lin S, Ke M, Zhang Y, Yan Z, Wu J. Structure of a mammalian sperm cation channel complex. Nature [Internet]. 2021;595(7869):746–50. Available from: http://dx.doi.org/10.1038/s41586-021-03742-6

56. Hwang JY, Mannowetz N, Zhang Y, Everley RA, Gygi SP, Bewersdorf J, et al. Dual Sensing of Physiologic pH and Calcium by EFCAB9 Regulates Sperm Motility. Cell. 2019;177(6):1480-1494.e19.

57. Chung JJ, Shim SH, Everley RA, Gygi SP, Zhuang X, Clapham DE. Structurally distinct Ca2+ signaling domains of sperm flagella orchestrate tyrosine phosphorylation and motility. Cell. 2014;157(4):808–22.

58. Zhao Y, Wang H, Wiesehoefer C, Shah NB, Reetz E, Hwang JY, et al. 3D structure and in situ arrangements of CatSper channel in the sperm flagellum. Nat Commun. 2022;13(1):1–15.

59. Qi H, Moran MM, Navarro B, Chong JA, Krapivinsky G, Krapivinsky L, et al. All four CatSper ion channel proteins are required for male fertility and sperm cell hyperactivated motility. Proc Natl Acad Sci U S A. 2007;104(4):1219–23.

60. Tamburrino L, Marchiani S, Minetti F, Forti G, Muratori M, Baldi E. The CatSper calcium channel in human sperm: Relation with motility and involvement in progesterone-induced acrosome reaction. Human Reproduction. 2014;29(3):418–28.

61. Rennhack A, Schiffer C, Brenker C, Fridman D, Nitao ET, Cheng YM, et al. A novel cross-species inhibitor to study the function of CatSper Ca2+ channels in sperm. Br J Pharmacol. 2018;175(15):3144–61.

62. Carlson AE, Burnett LA, del Camino D, Quill TA, Hille B, Chong JA, et al. Pharmacological targeting of native CatSper channels reveals a required role in maintenance of sperm hyperactivation. PLoS One. 2009;4(8).

63. Lishko P V., Botchkina IL, Kirichok Y. Progesterone activates the principal Ca2+ channel of human sperm. Nature. 2011;471(7338):387–92.

64. Strünker T, Goodwin N, Brenker C, Kashikar ND, Weyand I, Seifert R, et al. The CatSper channel mediates progesterone-induced Ca2+ influx in human sperm. Nature. 2011;471(7338):382–7.

65. Brenker C, Goodwin N, Weyand I, Kashikar ND, Naruse M, Krähling M, et al. The CatSper channel: A polymodal chemosensor in human sperm. EMBO Journal. 2012;31(7):1654–65.

66. Rahban R, Rehfeld A, Schiffer C, Brenker C, Egeberg Palme DL, Wang T, et al. The antidepressant Sertraline inhibits CatSper Ca2+channels in human sperm. Human Reproduction. 2021;36(10):2638–48.

67. Carlson EJ, Georg GI, Hawkinson JE. Steroidal Antagonists of Progesterone- and Prostaglandin E 1-Induced Activation of the Cation Channel of Sperm. Mol Pharmacol. 2022;101(1):56–67.

68. Carlson EJ, Francis R, Liu Y, Li P, Lyon M, Santi CM, et al. Discovery and Characterization of Multiple Classes of Human CatSper Blockers. ChemMedChem. 2022;17(15):1–15.

69. schierling-et-al-2022-synthesis-and-functional-characterization-of-novel-ru1968-derived-catsper-inhibitors-with-reduced.

70. Rehfeld A, Frederiksen H, Rasmussen RH, David A, Chaker J, Nielsen BS, et al. Human sperm cells can form paracetamol metabolite AM404 that directly interferes with sperm calcium signalling and function through a CatSper-dependent mechanism. Human Reproduction. 2022 May 1;37(5):922–35.

71. Luque GM, Schiavi-Ehrenhaus LJ, Jabloñski M, Balestrini PA, Novero AG, Torres NI, et al. High-throughput screening method for discovering CatSper inhibitors using membrane depolarization caused by external calcium chelation and fluorescent cell barcoding. Front Cell Dev Biol. 2023;11(January):1–14.

72. Lyon M, Li P, Ferreira J, Lazarenko R, Kharade S, Kramer M, et al. A selective inhibitor of the sper-specific potassium channel SLO3 impairs human sperm function. Proceedings of the National Academy of Sciences [Internet]. 2023;120(4). Available from: http://www.pnas.org/lookup/suppl/doi:10.1073/pnas.2216830120/-/DCSupplemental.https://doi.org/10.1073/pnas.2216830120

73. Latorre R, Castillo K, Carrasquel-Ursulaez W, Sepulveda R V., Gonzalez-Nilo F, Gonzalez C, et al. Molecular determinants of BK channel functional diversity and functioning. Physiol Rev. 2017;97(1):39–87.

74. Leonetti MD, Yuan P, Hsiung Y, MacKinnon R. Functional and structural analysis of the human SLO3 pH- and voltage-gated K+ channel. Proc Natl Acad Sci U S A. 2012;109(47):19274–9.

75. Tang QY, Zhang Z, Xia XM, Lingle CJ. Block of mouse Slo1 and Slo3 K + channels by CTX, IbTX, TEA, 4-AP and quinidine . Channels. 2010;4(1):22–41.

76. Mannowetz N, Naidoo NM, Choo SAS, Smith JF, Lishko P V. Slo1 is the principal potassium channel of human spermatozoa. Elife. 2013;2:1–19.

77. Brenker C, Zhou Y, Müller A, Echeverry FA, Trötschel C, Poetsch A, et al. The Ca2+-activated K+ current of human sperm is mediated by Slo3. Elife. 2014;2014(3):1–19.

78. Sánchez-Carranza O, Torres-Rodríguez P, Darszon A, Treviño CL, López-González I. Pharmacology of hSlo3 channels and their contribution in the capacitation-associated hyperpolarization of human sperm. Biochem Biophys Res Commun. 2015;466(3):554–9.

79. Wu F, Zhou Y, Li L, Shen X, Chen G, Wang X, et al. Computational Approaches in Preclinical Studies on Drug Discovery and Development. Front Chem. 2020;8(September).

80. Athanasiou C, Cournia Z. From Computers to Bedside: Computational Chemistry Contributing to FDA Approval. 2018;163–203.

81. Haddad Y, Adam V, Heger Z. Ten quick tips for homology modeling of high-resolution protein 3D structures. PLoS Comput Biol. 2020;16(4):1–19.

82. Prieto-Martínez FD, Arciniega M, Medina-Franco JL. Acoplamiento Molecular: Avances Recientes y Retos. TIP Revista Especializada en Ciencias Químico-Biológicas. 2018;21:65–87.

83. Rudrapal M, Egbuna C. Computer Aided Drug Design (CADD): From Ligand-Based Methods to Structure-Based Approaches. 1st ed. Elsevier; 2022.

84. Walters WP, Wang R. New trends in virtual screening. J Chem Inf Model. 2020;60(9):4109–11.

85. Hamza A, Wei NN, Zhan CG. Ligand-Based Virtual Screening Approach Using a New Scoring Function. Bone. 2012;23(1):1–7.

86. Khan SU, Ahemad N, Chuah LH, Naidu R, Htar TT. Sequential ligand- and structure-based virtual screening approach for the identification of potential G protein-coupled estrogen receptor-1 (GPER-1) modulators. RSC Adv. 2019;9(5):2525–38.

87. Maia EHB, Assis LC, de Oliveira TA, da Silva AM, Taranto AG. Structure-Based Virtual Screening: From Classical to Artificial Intelligence. Front Chem. 2020;8(April).

88. Rand M, Silva E, Hamil K. Non-Hormonal Male Contraception: A Review and Development of an Eppin Based Contraceptive. Pharmacol Ther. 2016;157(3):105–11.

89. Ayoub AM, Hawk LML, Herzig RJ, Jiang J, Wisniewski AJ, Gee CT, et al. BET Bromodomain Inhibitors with One-Step Synthesis Discovered from Virtual Screen. J Med Chem. 2017;60(12):4805–17.

90. Kyzer J, Noman M, Cuellar R, Chung S, Maitra S, Naqvi T, et al. Investigation of selective retinoic acid receptor alpha antagonist ER-50891 and related analogs for male contraception. Arch Pharm. 2023 Jan 16;e2300031.

91. Tao X, Mackinnon R. Molecular structures of the human slo1 k+ channel in complex with b4. Elife. 2019;8:1–27.

92. Lissabet JFB, Herrera Belén L, Lee-Estevez M, Risopatrón J, Valdebenito I, Figueroa E, et al. The CatSper channel is present and plays a key role in sperm motility of the Atlantic salmon (Salmo salar). Comp Biochem Physiol A Mol Integr Physiol. 2020;241(October 2019):110634.

93. Tejero R, Huang YJ, Ramelot TA, Montelione GT. AlphaFold Models of Small Proteins Rival the Accuracy of Solution NMR Structures. Front Mol Biosci. 2022;9(June):1–18.

94. Ritagliati C, Baro Graf C, Stival C, Krapf D. Regulation mechanisms and implications of sperm membrane hyperpolarization. Vol. 154, Mechanisms of Development. Elsevier Ireland Ltd; 2018. p. 33–43.

IX. Anexos

Carta de consentimiento informado para pacientes

"Análisis *in silico* e *in vitro* de moléculas con potencial uso de anticonceptivos masculinos sobre la funcionalidad del espermatozoide humano"

El presente estudio se encuentra bajo la supervisión de la Dra. Ana Alicia Sánchez Tusie, adscrita a la Facultad de Medicina de la Universidad Autónoma de Querétaro con dirección en Calle Clavel no. 200 Col. Prados de la capilla, Querétaro, Qro. Teléfono (442)1921200. Así mismo, este estudio será realizado por el responsable del proyecto: MC. Jorge Arturo Torres Juárez, estudiante del programa de Doctorado en Ciencias en Biomedicina de la Facultad de Medicina de la Universidad Autónoma de Querétaro.

Lo invitamos a tomar parte en un estudio de investigación en la Facultad de Medicina de la Universidad Autónoma de Querétaro, Campus Aeropuerto. Esta hoja de consentimiento puede tener términos médicos con los que usted no esté familiarizado, por favor siéntase libre de preguntar todo aquello que no entienda claramente.

Los métodos anticonceptivos son una solución clave para prevenir los embarazos no planeados. Sin embargo, la carga en este cuidado recae principalmente en la mujer, de tal modo que hace falta aumentar las opciones de anticonceptivos masculinos. De este modo, el objetivo del estudio es evaluar el efecto anticonceptivo de moléculas sobre la funcionalidad de los espermatozoides.

El presente estudio es un estudio experimental *in vitro* y tendrá un tiempo de duración aproximado de 40 minutos. En este estudio, los datos y la muestra pertinente del participante son tomados en una sola ocasión.

DESCRIPCIÓN DEL ESTUDIO.

Fase de evaluación inicial: Evaluar la historia clínica del participante, con especial atención a infecciones en los últimos 3 meses, diagnóstico de enfermedad venérea, lesión en la columna vertebral, uso de narcóticos y diagnóstico de diabetes.

Fase de pruebas fisiológicas: Obtención de la muestra de semen: Se dará un recipiente previamente rotulado, solicitando al participante proporcionar la muestra de semen en un cuarto privado ubicado en la proximidad del laboratorio.

Costo de las evaluaciones: La evaluación de la muestra de semen no tiene costo alguno para usted.

Beneficios: 1.- Los resultados de la muestra de semen, le permitirán conocer sus parámetros de calidad y funcionalidad de sus espermatozoides y la posibilidad de recibir recomendaciones de tratamiento en caso de ser necesarios. 2.-

Indirectamente, usted ayudará al desarrollo de métodos anticonceptivos masculinos.

Confidencialidad: La información que incluya su nombre, dirección u otros datos personales solo será registrada en el expediente del protocolo de investigación, el cual solo será consultado por los investigadores involucrados en el estudio. Si los resultados de esta investigación fueran presentados en artículos científicos, congresos o reuniones médicas y científicas, su identidad no será revelada. En caso de que los estudios o las evaluaciones llevadas a cabo durante el estudio, muestren hallazgos que se consideren de importancia para la evolución y/o tratamiento del cuadro clínico, se solicitará su autorización para ser comunicados a su médico tratante.

Participación voluntaria / suspensión de la participación: Su participación en este estudio es voluntaria. Puede rehusarse a participar o suspender su participación en el estudio en cualquier momento.

CONSENTIMIENTO INFORMADO: He leído la carta de consentimiento informado y entiendo de qué se trata el estudio. He hablado directamente con el responsable del estudio y ha contestado todas mis preguntas en términos que he podido entender. Puedo hacer cualquier pregunta en cualquier momento de la investigación. Recibí una copia de esta hoja de información.

ACEPTO VOLUNTARIAMENTE PARTICIPAR EN ESTE ESTUDIO.

Entiendo que puedo suspender mi participación en el estudio en cualquier momento sin que esto tenga consecuencias en mi relación con la institución. Mi identidad no será revelada en ninguna referencia del estudio o sus resultados. Además, recibí una copia de la carta de consentimiento.

Si tengo dudas o requiero información adicional respecto al estudio, puedo comunicarme con la Dra. Ana Alicia Sánchez Tusie ((442)1921200), Laboratorio de Biología Celular y Molecular de la Reproducción de la Facultad de Medicina de la Universidad Autónoma de Querétaro.

QUERÉTARO, **QRO**. DD_____, MM_____AÑO_____

Investigador (Nombre, Cargo y Firma):_____

En caso de suspender mi colaboración, autorizo que sigan utilizando mi información hasta que concluya la investigación:

Sí_____ **No**_____

Paciente (Nombre): _____
Firma:_____